Photoluminescence investigations of ZnO micro/nano structures

J. Rodrigues, N. Ben Sedrine, M. R. Correia, T. Monteiro*

Departamento de Física e i3N, Universidade de Aveiro, 3810 Aveiro, Portugal

*Corresponding author: tita@ua.pt

Abstract

Zinc oxide (ZnO) is probably one of the most researched wide bandgap semiconductors in the last decades due to its unique characteristics in terms of low production cost, high availability, bioinertness, and especially to its interesting optical properties. Even though this semiconductor is considered an "old" material and is known to possess such unique properties for more than three decades, the interest was renewed due to the advances in nanotechnology and the possibility to be produced in a vast number of nanostructures with tunable properties. An adequate knowledge of the nanomaterials' optical response is mandatory for assessing and optimize their functionalities towards different applications. Even thought, the PL properties of ZnO bulk materials have been know from several decades, a quite number of open questions remains, namely regarding the nature of defects responsible for the broad luminescence bands frequently observed in the visible spectral region, as well as the effects of reducing the dimensionality of the material to the nanoscale, since changes may arise due to the decisive role of the properties of surface/interface in the luminescence outcome. Indeed, the surface effects can strongly affect the nanostructure properties and can be used to tailor them, consequently having a profound influence on the performance of the devices where the nanostructures are employed. Hence, in this paper, an overview of the fundamental properties of ZnO, with emphasis on the main recombination mechanisms, both in bulk and at the nanoscale, is provided in order to disclose some of the current knowledge in this subject. Additionally, some examples of the myriad of applications where this semiconductor has been exploited are also discussed.

Keywords: ZnO; photoluminescence; recombination processes; surface states

Table of Contents

1. Introduction

Zinc oxide (ZnO), a II-VI semiconductor compound, is still one of the most studied wide bandgap materials worldwide due to its potential for a vast technical-scientific applications, ranging from optoelectronics to sensing devices [1–6]. In fact, such oxide host has already demonstrated its functionality in relevant domains, namely in gas sensing [7–10], piezoelectric devices [11,12], antibacterial and antifungal agents [13–15], transistors [16–18], etc. For several decades, this semiconductor has been used in its polycrystalline form, namely in paint pigmentation, sunscreens, facial powders, catalysts or even lubricant additives [1]. Even though the first reports on its characterization date from the early decades of the 20th century, it was in the end of the 1970s and the beginning of the 1980s that the research on ZnO reached its peak. However, the challenge in attaining *p*-type conductivity in a stable and reproducible way led to a stagnation [1–3]. In the mid-1990s ZnO research reawakened and ZnO emerged again as a promising wide bandgap semiconductor, which, together with gallium and related nitrides, revolutionized an increasing number of applications [3,4]. Even with some optoelectronic applications overlapping with that of gallium nitride (GaN), ZnO has some advantages among which are the availability of fairly high-quality ZnO bulk single crystals, much simpler crystal-growth technology, resulting in a potentially lower cost for ZnO-based devices. It is environmentally friendly, cheaper than the nitrides and is already produced by some 100 thousand tons per year [2,5]. Other favorable aspects of ZnO include its broad chemistry, its high energy radiation stability, biocompatibility and improved optical and electrical response, just to name a few [1,2,19]. The emphasis of this new active period of ZnO research was essentially promoted by the development of new growth techniques that enable the growth of epitaxial layers, quantum wells, quantum dots, as well as nanostructures with different shapes and sizes [3,20–23].

As mentioned above, one of the major drawbacks in using this material in optoelectronic applications is the lack of high quality, stable and reproducible *p*-doping, despite all the work devoted to this topic by numerous research groups [2,5,20]. A deep understanding of physical processes in ZnO is necessary in order to overcome this bottleneck, specifically regarding the nature of the residual *n*-type conductivity in undoped ZnO [2]. Thus, there are still a number of important issues to be addressed, where the nanostructures, as well as the formation of heterostructures and composite materials, offer a path to a new generation of devices, providing research material to "feed" the ZnO investigation.

With a bandgap energy (E_g) of ~3.4 eV at low temperature [5,24], this semiconductor oxide crystallizes, at ambient conditions, preferentially in the thermodynamically stable hexagonal modified wurtzite crystalline structure [1,5,25]. In such structure, each anion has four cations as nearest neighbors distributed in the corners of a tetrahedral arrangement (and vice versa), as a consequence of its hybrid sp^3 covalent bonding [1,5,25]. Moreover, and as happens in the II-VI compounds, the bonds are not purely covalent, revealing a substantial ionicity character [1]. The wurtzite structure (space group C_{6v}^4 symmetry in Schöenflies notation) can be described as an arrangement of two hexagonal closed packed (hcp) sublattices, each with one type of atom (Zn and O), shifted along the *c*-axis, with a slight deviation from the 1.633 value corresponding to the *c*/*a* ratio in the conventional hexagonal lattice [1,5]. In the case of ZnO, the *a* and *c* lattice parameters of the hexagonal cell unit have been reported as 3.2498 Å and 5.2066 Å [1,25],

respectively, corresponding to a *c*/*a* ratio of 1.6021. The internal displacement parameter in the conventional hexagonal cell *u*=(3/8)*c*, corresponds to ca. 0.382 in ZnO [1,25]. ZnO lacks of inversion symmetry and therefore a spontaneous and strain induced polarization develops in the wurtzite structure [1,25]. Additionally, ZnO crystals exhibit polar surfaces, being the most common the (0001) basal planes, depending on the opposite Zn^{2+} and O^{2-} charged ions. Such behavior have a strong influence on the semiconductor properties, as is the case of growth speed, etching rates and defect generation [1,5,25].

The knowledge of the electronic band structure of a given semiconductor is of paramount importance to understand the material's optical recombination processes. The bulk ZnO is a direct bandgap semiconductor, with the conduction band (CB) minimum and the valence band (VB) maximum occurring at the same $\vec{k}$ located at Brillouin zone center where $\vec{k} = \vec{0}$ [1,25,26]. The VB maximum is built by *p*-atomic electronic states combined with *d*-atomic levels. Under the effect of the crystal field and spin-orbit interaction, the VB splits into three Kramers levels labelled by A, B and C with Γ_7, Γ_9, Γ_7 symmetry in the double group notation, respectively [27,28] (see Figure 1). Since the CB has Γ_7 symmetry, reflectivity measurements evidence that resonance features from A and B free excitons appear for $\vec{E} \perp \vec{c}$, whereas the C peak occurs for $\vec{E} || \vec{c}$ [29]. According to the selection rules, $\Gamma_7 \rightarrow \Gamma_9$ transitions are allowed when light is oriented in a way that $\vec{E} \perp \vec{c}$, while the $\Gamma_7 \rightarrow \Gamma_7$ transitions are permitted for both polarizations (perpendicular and parallel) [30]. The energy separation of the A and B electronic states has been reported as 4.9 meV [27,31], whereas 43.7 meV corresponds to the energy difference between B and C [1].

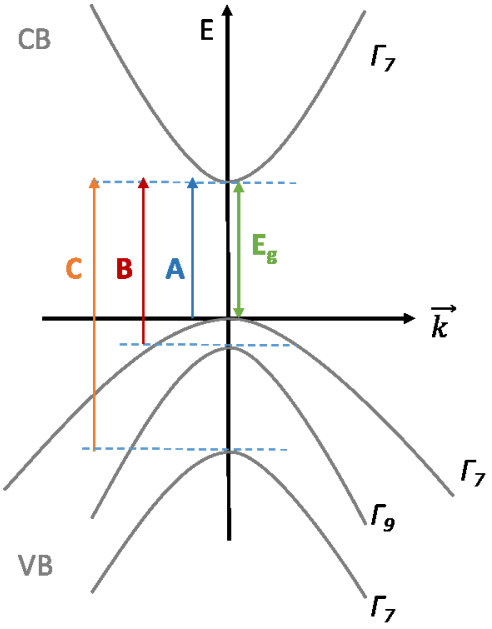

Figure 1 – Schematic representation of the conduction (CB) and valence (VB) bands symmetries near the high-symmetry Γ point ($\vec{k} = \vec{0}$) and their spectral ordering (adapted from [1,27]).

The bandgap energy of a given semiconductor is known to decrease with increasing temperature. The thermal lattice expansion and electron-phonon interaction [32,33] result in a shrinkage effect of the fundamental bandgap that can be (in first approximation)

described by a parabolic dependence on temperature, known as the empirical Varshni law [34],

$$E_g(T) = E_g(0) - \frac{\alpha T^2}{\beta + T} \qquad \textit{Eq. (1. 1)}$$

where $E_g(0)$corresponds to the bandgap energy at 0 K, T is the absolute temperature, and α and β are the temperature parameters. β is proportional to the Debye temperature, θ_D (399.5 K [25]), being approximately the same value at low temperatures [35] and assuming a value ca. $\frac{3}{8}\theta_D$ for $T > \theta_D$ [36]. For bulk ZnO, the dependence of the excitonic bandgap energy measured by photoluminescence (PL) experiments using Eq.(1) results in values α and θ_D, that differ from each other by ~18% and 4% ($\alpha = 6.7 \times 10^{-4}$eV/K and $\theta_D = 672$ K or $\alpha = 8.2 \times 10^{-4}$eV/K and $\theta_D = 700$ K, as reported by Boemare *et al.* [32] and Wang *et al.* [37], respectively).

The wurtzite structure exhibits four atoms per unit cell, resulting in twelve phonon modes at the Brillouin zone center, corresponding to the following phonon branches: one longitudinal acoustic (LA), two transverse acoustic (TA), three longitudinal optical (LO), and six transverse optical (TO) [1,38]. Since the wurtzite crystal structure belongs to the C_{6v}^4 spatial group, the group theory predicts eight sets of phonon modes at Γ-point with irreducible representation $\Gamma = \Gamma_{ac} + \Gamma_{opt} = 2A_1 + 2E_1 + 2B_1 + 2E_2$, where Γ_{ac} and Γ_{opt} stand for acoustic and optical modes, respectively [39]. A_1 and B_1 are nondegenerate modes while E_1 and E_2 are doubly degenerated [38]. One set of A_1 and E_1 modes correspond to acoustic phonons, whereas the remaining ones are optical modes, $\Gamma_{opt} = A_1 + E_1 + 2B_1 + 2E_2$ [38–40]. A schematic representation of the atomic displacement of the optical modes present in the wurtzite structure is depicted on Figure 2. Among these vibrational modes, only the A_1, E_1 and E_2 are Raman active. A_1 and E_1, due to their polar character, are also infrared (IR) active and B_1 are neither Raman or IR active and are called silent modes [38–40]. The two nonpolar Raman active E_2 branches, E_2^{low} and E_2^{high}, are associated with the vibrations of the Zn and O sub lattices, respectively [25]. Since the wurtzite structure is an anisotropic noncentrosymmetric crystal, the crystal field leads to the polarity-induced splitting of the optical E_1 mode at Γ into TO and LO branches due to the macroscopic electric field [38]. A similar effect occurs for the optical A_1 mode, showing different frequencies near the Γ-point, which depend on the symmetry direction [38]. Thus, the A_1 and E_1 polar modes exhibit different energies for the LO and TO polarizations. In both cases, the LO phonon frequency exceeds that of the TO mode. Due to this frequency split of polar modes into LO and TO, a higher number of eigenfrequency values arises in comparison to those predicted by group theory [5]. As for the case of the electronic band structure, the knowledge of the vibrational modes assumes an important role on the analysis of the optical properties of the ZnO structures. The typical phonon energies found for the first-order Raman modes of ZnO are listed in Table 1 [39]. Figure 3 shows a typical Raman spectrum recorded for ZnO microrods produced by the laser-assisted flow (LAFD) deposition approach.

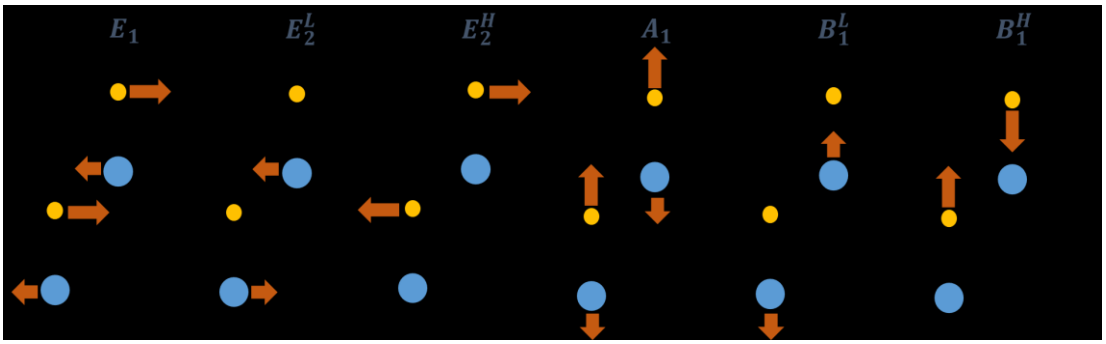

Figure 2 – Atomic displacement of optical phonon modes in the wurtzite structure. H and the L superscripts correspond to high and low frequency modes, respectively. Adapted from reference [40].

Table 1 – Typical phonon energies at the zone center ($\vec{k} = \vec{0}$) of wurtzite ZnO at room temperature [39].

	E_2^{low}	$A_1(TO)$	$E_1(TO)$	E_2^{high}	$A_1(LO)$	$E_1(LO)$
Energy (cm^{-1})	99	378	410	438	574	590

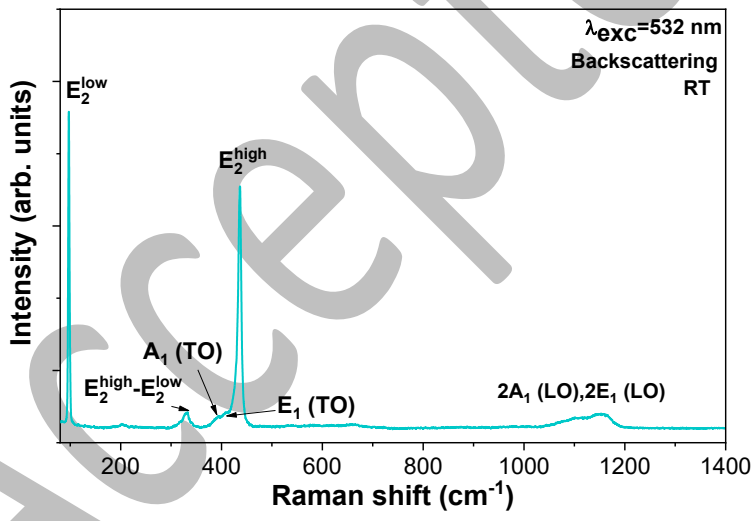

Figure 3 – Representative Raman spectrum obtained for ZnO microrod samples prepared by the laser-assisted flow deposition method. The spectrum was acquired at room temperature under 532 nm laser line excitation under backscattering configuration.

The ZnO properties mentioned up to this point correspond to the semiconductor in its bulk form. However, changes may arise by reducing the dimensionality of the material to the nanoscale. Not only the reduction in the spatial dimension at a particular direction can introduce quantum confinement effects, but also the increase in the surface-to-volume ratio may have a tremendous impact on the semiconductor physical properties. In the case of ZnO, the exciton Bohr radius is ~1.8 nm [41,42], meaning that for most nanostructures quantum confinement effects can be neglected when compared with bulk material. Therefore, the influence of the surface becomes the most relevant factor that rules the changes observed at the nanoscale.

The ZnO possesses one of the richest varieties of nanostructures, exhibiting a diversity of morphologies, which can be produced by uncountable methods. In this way, it is possible to obtain morphologies that maximize the surface-to-volume ratio, which is of particular importance for several applications, namely in the sensing or photocatalysis fields. With the increase of the surface area over the volume, surface effects tend to dominate the crystal properties and new optical features may arise. These surface states can be due to dangling bonds, point defects or adsorbed species at the ZnO surface [43]. In the presence of such states, the Fermi level is pinned at the surface, which causes a bending of the electronic bands in the proximity of the surface, leading to the capture of charge carriers in that region, and the generation of a surface charge [43–45]. This bending will be determined by the charge distribution at the surface and its effects of the materials' properties will depend on the size of the nanostructures. There is a critical diameter that leads to a full depletion of the structures, with a surface barrier height on the order of the surface-pinned Fermi level. Fully depleted samples exhibit an insulating character and strongly inhibit the recombination of carriers from the bulk, since a potential barrier is formed either for electrons and/or for holes [44]. On the other hand, if the defects introduced by the surface states are optically active, new luminescence features will arise, dominating over the bulk luminescence. It is also important to bear in mind that the crystallographic orientation of the surface may promote the formation of different types of defects, and thus with different implications to semiconductor properties [44].

Low dimensional ZnO nanostructures with "custom-made" geometries as building blocks are expected to play a decisive role in the fabrication of nanodevices [46,47]. 1D ZnO nanostructures, namely nanorods and nanowires, have been subject to intense research due to their excellent properties, mostly associated to their large surface area/volume ratio [47]. Additionally, tetrapodal-like structures have attracted some attention due to their unique electronic transport properties, demonstrating higher electron transfer efficiency when compared with the nanorods [48–51]. Furthermore, the branching structure provides a large surface area for sensing purposes and charge separation, while the good interconnection between the branches offers multiple pathways for electron transport [52,53].

For a wider comprehensive review of the ZnO physical properties please refer to the work of references [1,2,5,25].

2. Recombination processes

ZnO is probably one of the most scrutinized semiconductors from the point of view of its optical properties, particularly regarding its luminescence output. When light interacts with a semiconductor, different phenomena may occur, namely the photogeneration of electron-hole pairs that may subsequently recombine radiatively, giving rise to the material's PL spectra, which is strongly dependent on the optical excitation photon energy. Additionally, the measured spontaneous emission also depends on the nature of the semiconductor, namely regarding its intrinsic character or the preence of foreign impurities. Any perturbation on the material lattice periodicity, the so-called defects, may change dramatically the luminescence outcome of the semiconductor. Several lattice imperfections can coexist in a given host, such as punctual (native and contaminant impurities), extended and surface defects, being extremely conditioned by the used growth method [54–58]. Moreover, most of the device applications, dealing with semiconductors, require controlled and reproducible doping procedures to incorporate

foreign species (impurities) in the host materials to promote/enhance properties like metal-like conductivity or visible light absorption, for instance. Additionally, complex defects may also be formed by the interaction of the different types of defects present in the same sample [59–62]. Some of them may be optically active, resulting in both narrow and broad PL features, covering the ultraviolet, visible and near infrared (UV-VIS-NIR) spectral range. In the following section, we will briefly review some of the most common optical recombination processes contributing to the PL spectra of ZnO bulk and micro/nanostructures.

2.1 Bulk material

2.1.1 Near band edge recombination

When a semiconductor material is irradiated with photons with energy equal or higher than the material's bandgap, electron and hole carriers are photogenerated. In undoped high purity crystals and owing to the Coulomb interaction between the electron and hole, free excitons (FX) can be formed. In that case, the electron and hole remain bound to each other as a hydrogen-like system, mediated by the dielectric constant of the material. Such elementary excitation is free to travel through the material lattice covering several lattice constants [63]. For direct bandgap materials, as is the case of ZnO, their radiative recombination arises at energies [63,64]

$$\hbar\omega = E_g - E_X - n\hbar\omega_{LO} \qquad \textit{Eq. (2. 2)}$$

where E_X denotes the *Wannier-Mott* [65] FX binding energy, which corresponds to the energy required for the exciton dissociation and $n\hbar\omega_{LO}$ denotes the optical phonons assisting the transition, designated by vibronic replicas. If the transition occurs without the participation of phonons, the narrow line is called zero phonon line (ZPL) [66]. However, in polar materials most of the PL processes are assisted by LO phonons with the electron-phonon interaction quantified by the Huang-Rhys factor (S) [66,67].

As mentioned in the introduction, three types of FX can be distinguished in ZnO, depending on whether the hole resides in the A, B, or C valence bands [1,27,28,68]. The ZnO FX binding energy is one of the largest ones reported for wide bandgap semiconductors (~ 60 meV against the ~25 meV of GaN) [2,58]. Several authors using different spectroscopic techniques [1,2,29,69,70] have experimentally measured the energy of FX transitions. For instance, the values for the ground state ($n = 1$) recombination for ZnO with natural isotopic composition using reflectivity measurements at 8 K were reported by Tsoi *et al.* [68] as 3.3760 eV, 3.3813 eV and 3.4213 eV for the A, B and C excitons, respectively.

Typically, the semiconductor crystals also present a number of defects and impurities that can bound these FXs, forming the so-called bound exciton (BX) complexes [31,69,71–74]. When donor and acceptor species are not ionized, the bound excitons are labeled as D^0X and A^0X, respectively. As a consequence of its localization, the photon emitted in the recombination of a bound exciton is [65],

$$\hbar\omega = E_g - E_X - E_{loc} - n\hbar\omega_{LO} \qquad \textit{Eq. (2. 2)}$$

spectrally located at lower energy than that of the FX recombination. E_{loc} corresponds to the localization energy of the exciton in the impurity/defect. The observation of such transitions represents an important optical indication of the presence of impurities in the crystals.

Figure 4 shows the temperature-dependent PL spectra of a bulk ZnO sample in the near band edge (NBE) spectral region. At low temperatures (14 K), one observes an extremely low intensity of the FX recombination, followed at lower energies (~3.36 eV) by the vibronically assisted (by ca. 72 meV LO phonons) D^0X recombination lines (the I_i lines as mentioned by Thonke *et al*. [27,75]). Some of these sharp lines were already attributed to the presence of impurities, as is the case of H, Al, Ga, and In, as reported by Meyer *et al*. [71], however, others were not yet identified. Additionally, on the low-energy side of the bound exciton lines (ca. 40 meV apart from the D^0X lines [5,75]), the recombination processes have been attributed to the two-electron satellite (TES) lines that correspond to radiative recombination of a D^0X which leaves the donor in an excited state [2]. The donor binding energy, E_D, can be estimated by the Haynes rule, which establishes a linear relationship between the localization energy of the exciton and E_D [5]. The low temperature spectrum also exhibits a line at 3.33 eV which has been tentatively assigned to structural defects [5,76]. As the temperature increases the relative PL intensity decrease due to the D^0X dissociation, and at RT the emission is dominated by the FX recombination peaked at 3.28 eV.

Besides the FX and D^0X transitions, many semiconductors exhibit free-to-bound radiative recombination processes (*e.g.* (e, A^0) where a free electron recombines with a hole trapped at a neutral acceptor) and band to band transitions, which are favored temperatures higher than the room temperature. In the case of free-to-bound recombination the energy of the emitted photon is given by [65],

$$\hbar\omega = E_g - E_A - n\hbar\omega_{LO} \qquad \textit{Eq. (2. 3)}$$

where E_A is the binding energy of the hole to the acceptor. The line shape of a band-to-band transition is known to be proportional to the joint density of states and Fermi distribution function [65]. It is worth to mention that the above mentioned transitions are also strongly sensitive to strain effects and concentration doping, which can, for instance, influence their width and peak position [77–79].

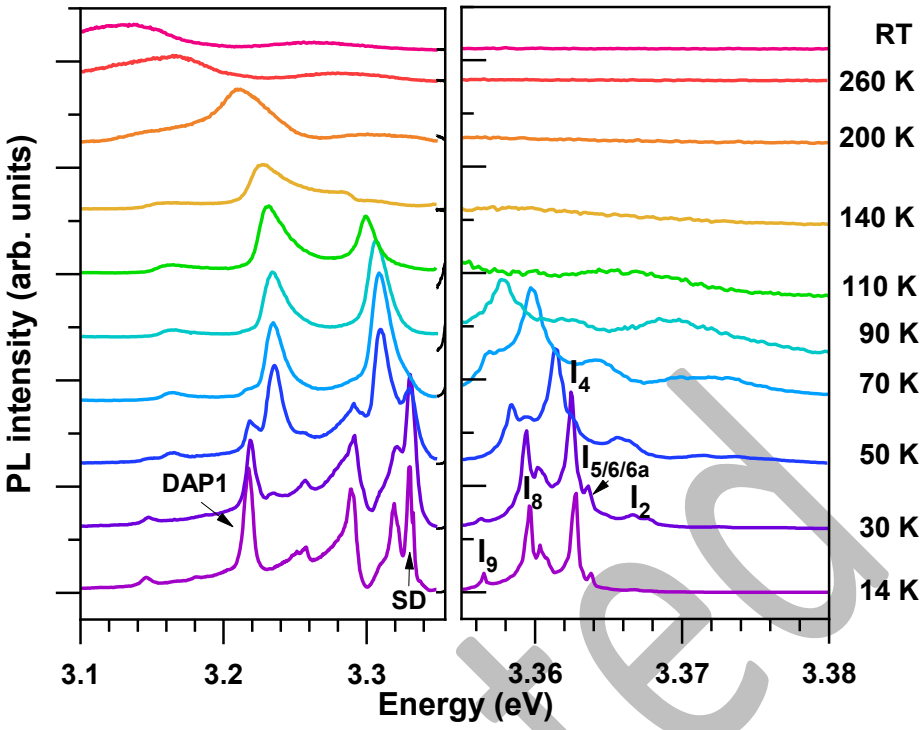

Figure 4 – Temperature-dependent near band edge PL spectra of bulk ZnO provided by Eagle-Picher Technologies (grown by seeded chemical vapor transport). Lines labelled according reference [72]. "SD" stand for structural defect. Data adapted with permission from AIP Publishing [72].

Besides the aforementioned optical transitions, many semiconductors exhibit the so-called donor-acceptor pair (DAP) transitions, as highlighted in Figure 5. In this case, donor and acceptor species are simultaneously present in the material and the resulting radiative recombination is due to the overlap of the wavefunctions of an electron in a donor with a hole in an acceptor. The emission resulting from the DAP recombination has an energy of [63,65],

$$\hbar\omega = E_g - E_D - E_A + \frac{e^2}{4\pi\varepsilon_0\varepsilon_r r_{DA}} - n\hbar\omega_{LO} \qquad \textit{Eq. (2. 5)}$$

where E_A and E_D are the acceptor and donor binding energies, respectively. The last term in Eq. 2.5 before the LO vibronic progression describes the Coulombic interaction between donors and acceptors, with r_{DA} being the distance between the donor and the acceptor for a particular pair, e is the electron charge, ε_0 is the permittivity of free space and ε_r is the semiconductor dielectric constant [63,65]. Therefore, and as was well explained by Dean *et al*. [80], the energy transition of DAP optical centers depends if the carriers are trapped by nearby or distant donors and acceptors in lattice sites, resulting in high and low energy transitions. An experimental consequence of this is, *e.g.* that the spectral position of the DAP PL transitions depends on the excitation density. Higher excitation densities promote the population of a higher number of donor and acceptor states and, consequently, there is a higher probability of having close-by recombination partners, which is transduced in the observation of higher energy PL signals associated to these recombination. For instance, in the case of ZnO layers intentionally doped with

nitrogen, Zeuner *et al.* [81,82] reported a broad line peaked at 3.235 eV followed by LO-phonon replicas which has been assigned to a DAP emission, involving the substitutional nitrogen (N_O) acceptor. An activation energy of 165 meV for the N_O acceptor was estimated from PL experiments [83].

The activation energies for the nonradiative processes that compete with the radiative luminescence can be estimated from the temperature-dependent PL spectra. Usually, narrow emission lines can be fitted to Lorentzian line shapes (Gaussian line shape in the case of broad emission bands). Assuming that the nonradiative processes are negligible at low temperatures, the PL intensity at a finite temperature, $I(T)$, can be generally calculated by the Arrehnius equation [67,84],

$$I(T) = I(0)[1 + C\ exp(-E_a/k_BT]^{-1} \qquad \textit{Eq. (2. 4)}$$

where $I(0)$ accounts for the PL intensity at 0 K, E_a is the activation energy for the nonradiative process, k_B is the Boltzmann constant and C is the pre-exponential factor that accounts for the degeneracy of the involved electronic levels.

2.1.2 Deep level emission

Figure 5 shows typical low temperature PL spectra of two different bulk samples (provided by Tokyo Denpa and CrysTec, both grown by hydrothermal methods). Besides the aforementioned transitions in the near band edge region, deep level emissions peaked in the visible spectral range are also observed. Although other emission bands in the blue, yellow and orange/red spectral region have also been reported [2,85–87], the most scrutinized deep level emission in ZnO corresponds to the green luminescence (GL) peaked ca. 2.4 eV [1,2,25]. Even so, there is still some controversy regarding the nature of the different defect emissions in that region and different hypotheses have been proposed to explain them [2,54,88–93]. Among those, the most common origins for this defect-related luminescence account for intrinsic defects in the ZnO matrix, namely oxygen/zinc vacancies (V_O/V_{Zn}), Zn antisites (Zn_O), interstitial Zn atoms (Zn_i), transitions from Zn interstitials to Zn vacancies and extrinsic impurities, as is the case of Cu [92–94].

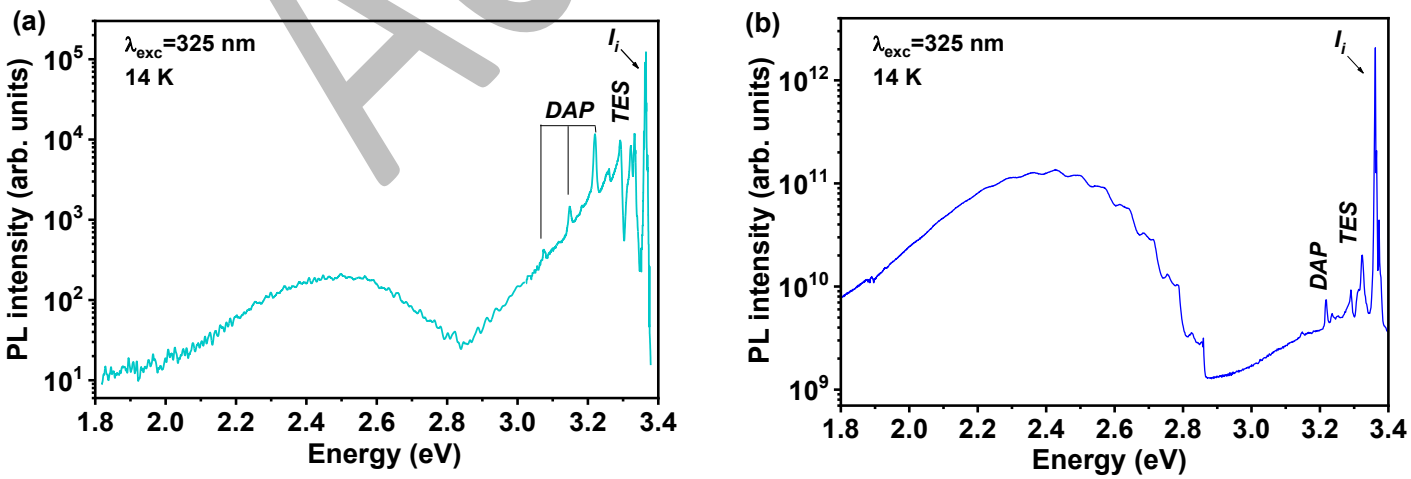

Figure 5 – 14 K PL spectra of bulk ZnO obtained upon above bandgap excitation (325 nm), showing the (a) unstructured (sample from Tokyo Denpa) and (b) structured (sample from CrysTec) green luminescence band.

The GL often exhibits distinct spectral shapes depending on the type of samples and their growth methods. In some cases, a structured GL is observed, which is commonly attributed to Cu_{Zn} related-defects. This band is known since the 60's and was extensively studied by Dingle [92]. As reported by Kuhnert and Helbig [95], the structure of the GL can be well accounted by a vibronic progression of 72 meV-LO phonons and the emission can be well described using the coordinate configuration model using the Born-Oppenheimer approximation and considering a Huang-Rhys factor of S~6.5 [1]. Here, the intensity of the n-th phonon replica is given by [96],

$$I_n \; \alpha \; e^{-S} \frac{S^n}{n!} \qquad \textit{Eq. (2. 6)}$$

Nonetheless, a structureless band reported at nearly the same position as the structured one is often associated with other defects, namely V_O or V_{Zn} [2]. Thus, in spite having similar peak positions and widths, the origin of the observed GL may be rather different from sample to sample [1,2]. Indeed, it is known that different types of defects may be responsible for broad luminescence emission in this spectral range. Moreover, the observed broad bands frequently result from the overlap of multiple transitions from distinct optical centers, with the peak position of the overall band misleading the actual energy position of the emitting centers and hampering a clear correlation between the observed emission and the defects present in the analyzed crystal [97]. Additionally, the formation of these defects is strongly dependent on the growth methodology, as well as post-growth processing [54,55,57]. For instance, the formation energy of the oxygen vacancy is strongly dependent on the availability of Zn and O atoms during the growth process [55]. All these issues make the association between a specific defect and its corresponded radiative recombination in this (and any other) spectral region a tremendous challenge and, as so, an unambiguous correspondence has not been yet effectively settled [2,54,88–91]. As examples, should be highlighted the work of Meyer *et al.* [98,99], where these authors performed both PL and optically detected magnetic resonance (ODMR) studies on undoped commercial ZnO single crystals from Eagle-Picher and evidenced that for those samples the unstructured GL was associated with oxygen vacancy defects. On the other hand, Janotti and Walle [55] carried the first-principles investigations on native point defects in ZnO based on the density functional theory and conclude that the oxygen vacancy has an high formation energy, thus being less likely to form and not contributing to the GL. These authors suggest zinc vacancies as a possible source of the mentioned emission. However, Wang *et al.* [60] claimed that neither the zinc nor the oxygen vacancies are responsible for the green emission in the samples analyzed by them. Their conclusion were based on ODMR studies performed on different commercial ZnO bulk single crystals nominally undoped (from Tokyo Denpa and Cermet Inc. providers). They showed a direct correlation between the presence of Zn vacancies and the radiative transitions related to the red PL emission, but not with the green one. Therefore, care must be taken with the assignment of the radiative transitions to a given defect simply by comparing with the literature reports. Complementary techniques are often necessary to assess the chemical nature of an optical center, and even then the analysis may not be straightforward.

In spite of less common reported, the visible emission bands in the blue, yellow and orange/red spectral regions observed for bulk samples, they have been also attributed to native defects in the ZnO. This attribution results from the fact that even high quality ZnO crystals are known to possess relatively high density of native defects contributing to the visible luminescence [87,97,100–102]. Indeed, even the defects indicated as the origin of

the GL have been also associated with the transition in the remaining visible region, either as single point defects or by forming complex with other defects. In fact, that is the case for both yellow and orange/red bands, which have been connected to the same deep defect level, however originating from different initial states [2,87]. The Zn vacancy and related complexes are amongst the most popular assignments for such emissions [97,103], which is not surprising since the Zn vacancy has one of the lowest formation energies [55]. According to Chai *et al.* [104], for such defect three peaks located at ~414 nm (~2.99 eV), 525 nm (~2.36 eV) and 600 nm (~2.07 eV) can be identified, being linked with different charge state transitions. Such relation was corroborated by the theoretical work of Sokol *et al.* [105], where these authors investigated intrinsic point defects in ZnO by means of embedded cluster hybrid quantum mechanical/molecular mechanical calculation approach. Their results demonstrated that Zn vacancies originate the major acceptor in ZnO and that this defect is found to be stable in five different charged states, responsible for PL bands in the ultraviolet (DAP transition involving an acceptor level at 3.2 eV); green (triplet level at 2.5 eV) and red (1.9–2.0 eV). Moreover, they affirmed that neutral oxygen interstitials might also contribute to blue and green PL emission by an exciton recombination and DAP transition from donor Zn interstitials, respectively. On the other hand, as already reported by others, the same authors claimed that oxygen vacancies are not responsible for the green luminescence, but could play a role in the UV and red-orange luminescence bands (at 2.1 eV and below) through an exciton recombination mechanism [105].

The presence of impurities may also account for transitions in the visible spectral regions. As an example, Li impurities have been reported as deep acceptors in ZnO, giving rise to a broad emission in the yellow region [2]. Additionally, substitutional nitrogen ions in the oxygen sites have also been indicated as a deep acceptor, resulting in transition in the red [2,104]. In the case of the already mentioned involvement of Cu impurities in the structured GL, according to Sokol *et al.* [105], calculated defect levels of this impurity at 2.7 eV and 0.55 eV were obtained, in line with experimental results, thus establishing Cu as an additional source of green luminescence in ZnO. Still, a great number of the defects in ZnO structures remain undisclosed and therefore, how their optical signatures may influence the overall PL spectra of ZnO [87].

2.2 Micro and nanostructures

Up to now, only the luminescence properties of the bulk samples were discussed. However, as mentioned in the Introduction, when the size of the ZnO structures is reduced (increasing their surface-to-volume ratio), the surface and interface properties will have a higher influence on the luminescence outcome, even dominating it. At the surface of a crystal, there is a break in the periodicity of the crystal lattice, thus leading to the appearance of dangling bonds on surface atoms. The presence of these non-terminated bonds promotes the adsorption of additional atoms/molecules. As such, the surface atoms can be seen as a kind of defect and the anisotropy of the crystals determines that different kinds of crystal surfaces have different defects [106].

It is well accepted that the surface effects and the formation of the depletion region is responsible for a surface band bending, which have a profound effect on the PL of ZnO. Still, the mechanism how the surface effects influence the PL is under debate and strongly depends on the surface-to-volume ratio of the nanostructures, as well as on the type of species and charges in the neighborhood of the surface [107]. It is known that the presence

of point defects at the surface of the semiconductor, such as oxygen or zinc vacancies, can act as adsorption sites for some chemical species [108]. For instance, when samples are produced and stored in air ambience, the surrounding environment will provide a source of acceptors/donors species at the surface of the semiconductor (*e.g.* O_2 molecules), which will contribute with additional charges to the surface. Therefore, the position of the Fermi level at the surface will be controlled by the charge induced by the adsorbates [109]. When species like O_2 or OH are present at the ZnO surface, they tend to act as acceptors, trapping negative charges at the surface states and thus reducing the free carrier density in that region [110,111]. By increasing the amount of negative charges at the surface/interface of the semiconductor, the electrons need to overcome a potential barrier to reach the surface (from the bulk), forming a depletion region. With the formation of such a space charge region, the Fermi level becomes pinned at the surface of the semiconductor, leading to upward band bending near the nanostructures surface [44,110,112,113], as schematized on the left side of Figure 6. Assuming a band bending as the one depicted in Figure 6, the electrons are likely to be located in the inner (bulk) part of the structures, whereas holes tend to move to the surface [112]. In this case, the spatial separation of the carriers may reduce or even hinder the radiative recombination between the energy bands of the semiconductor, and the surface-related recombination processes will dominate the PL spectra. Thus, for sizes and morphologies with a large volume when compared to the surface area, this effect may be limited and almost negligible. However, if the surface-to-volume ratio is high, the surface-related states will have the highest contribution to the PL spectra, if these defects are optically active. Thus, new emission may arise, dominating over the bulk luminescence.

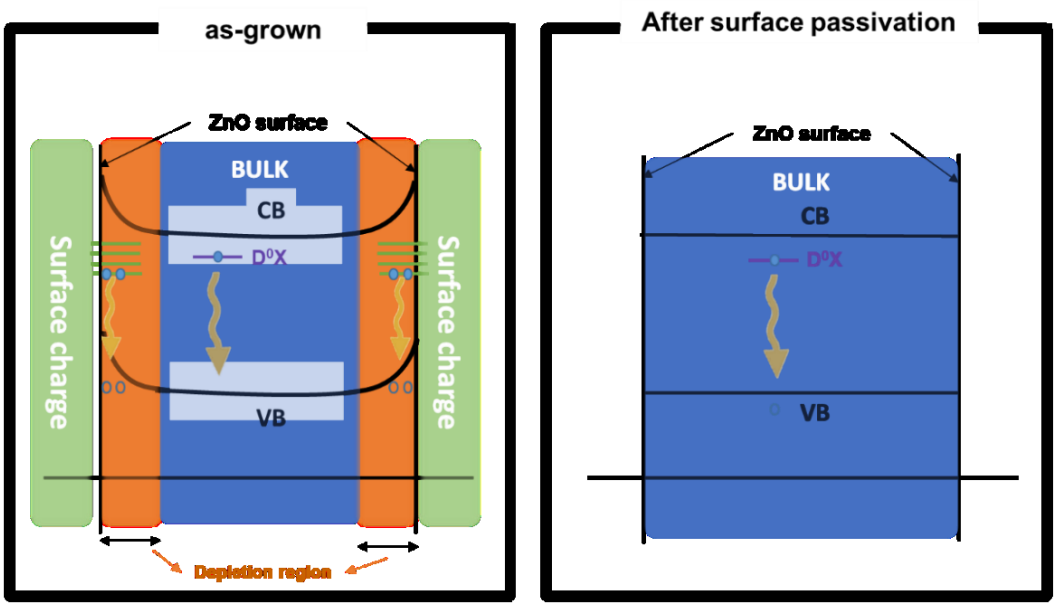

Figure 6 – Schematic representation of the effect of the surface passivation treatment on the energy band diagram of the ZnO microrods. (Image adapted from the work reported in reference [43].)

As so, the distribution of the surface *vs* the bulk defects will play a key role in tailoring the properties of the semiconductors, and consequently on the devices' performance [114]. Indeed, the influence of the surface in the PL emission brought further variables to the discussion regarding the origin of the different optical centers. In the last two decades, the group of Djurisic *et al.* [54,115–119] have made an extraordinary contribution to the discussion of the nature of the visible broad bands in different types of ZnO nanostructures. They studied several ZnO nanostructures produced by a variety of methods and observed that the production methodology was critical for the luminescence

response. As stated above for the bulk samples, the orange-red emissions are frequently assigned to defects related to excess oxygen, even in the case of the nanostructures. Tam *et al.* [116] showed that for their nanorods produced by the hydrothermal method, the annealing treatments in air resulted in a prominent red emission, as well as higher O_1/O_2 and O_1/Zn ratios measured by XPS. O_1 corresponds to oxygen ions in the wurtzite ZnO structure, and O_2 is usually assigned to loosely bound oxygen on the surface, namely as OH groups or O^{2-} ions in oxygen deficient regions. An O_1/Zn lower than 0.5, as the one obtained in that work, means oxygen deficiency in the bulk of the rods. As such, Zn vacancies or vacancy complexes should not be involved in the red emission depicted by those structures. Moreover, the persistence of the emission for annealing treatments up to 600 °C points to the possible involvement of defect complexes, even though their chemical nature was not assessed. Since the orange-red emission was enhanced after annealing under oxygen-rich conditions in similar samples [54], its association with excess oxygen prevails as the most accepted origin for such defect emission.

ZnO nanorods synthesized by the hydrothermal method in different substrates revealed the presence of the yellow-orange defect luminescence, besides the NBE recombination peaked in the UV spectral region [54,120]. The authors performed several post-growth treatments at different atmospheres (air, argon, nitrogen and forming gas (dissociated ammonia atmosphere, $H_2 + N_2$)) and at different temperatures (200 °C, 400 °C, and 600 °C). They observed that annealing in air at temperatures higher than the 200 °C resulted in an increase of the PL intensity of the defect-related emission, as well as the rise of the red and near infrared components. As both yellow and red emission bands had been previously assigned to defects related to excess oxygen [115,120–122], annealing treatments at distinct controlled atmospheres enabled to explore that hypothesis. As such, annealing at 600 °C in argon, forming gas ($H_2 + N_2$) or nitrogen resulted in a reduction of visible emission, thus corroborating the link with excess oxygen, particularly in interstitial positions [120]. In line with these results, Hsu *et at.* [123] also reported the growth of ZnO nanorods via a solution-based method, which exhibited a strong yellow-orange emission band attributed to bulk defects associated with excess oxygen. The authors also conducted annealing treatments in forming gas (at 450 °C for 30 min to 2 h) and observed the suppressing of the yellow-orange luminescence and the enhancement of the NBE recombination. If excess oxygen (*e.g.* oxygen interstitials) is in the origin of this emission, annealing in a reducing atmosphere should eliminate such defects and the yellow emission should vanish from the PL spectra, which was indeed demonstrated [123]. Moreover, similar ratios of yellow-orange defect luminescence *vs* the NBE one were observed for nanorods with different diameters (~30 – 50 nm *vs* 100 – 200 nm) and the cathodoluminescence (CL) spectra for individual nanorods is analogous to what is detected for a bundle of rods. As so, the authors concluded that the recorded emission should arise from the bulk and not from the surface of the ZnO structures [123].

Nevertheless, in the case of samples produced by the hydrothermal method the yellow emission (at ~2.15 eV) has also been associated with surface capping by zinc hydroxide [54,124], that disappears after annealing. As both water and hydroxyl groups can be desorbed with increasing temperature, the yellow emission may originate from the presence of $Zn(OH)_2$ or hydroxyl groups adsorbed at the surface of ZnO, instead arising from above mentioned interstitial oxygen [54]. Indeed, previous studies performed on ZnO synthesized in hydrothermal conditions also pointed out to surface mediated processes, since photodegradation of the yellow luminescence band was observed as a function of increasing photon illumination time, as well as a dependence of the recombination degradation on the material's environment [23]. In the same work, after

thermal annealing (150 °C, 12 h), an overall shift of the luminescence to higher energies was recorded due to the contribution of a developed/enhanced green component, exhibiting an overlap of at least two emitting centers, the green and yellow/red luminescence bands.

According to the works of Djurisic and others [54,91,115,118], the green emission is more commonly displayed by samples prepared via thermal evaporation approaches and was seen to be strongly dependent on the surface. In the case of the tetrapod samples prepared by oxidation of Zn (in humid argon and dry nitrogen flow) [115], which exhibited the GL, coating the structures with surfactants led to a pronounced reduction of the green emission, strongly suggesting that the defects responsible for such emission are located at the surface [54,115]. This was further corroborated by coating the surface of the ZnO structures with KCl or KI crystals, which also resulted in the suppression of green luminescence. Additionally, applying the same surface treatment to the samples produced by chemical route, which presented the yellow emission, did not affect the intensity of the PL signal. In fact, only a slight redshift of the peak position was observed, likely related to the suppression of the green component of the overall emission [115]. As no significant changes were observed in that case, the authors concluded that the centers responsible for the yellow band were not located on the surface [115]. In fact, structures prepared by similar thermal evaporation procedures, as the ones reported in [118], also exhibited a tetrapodal shape, with slightly different sizes ratios depending on the growth atmosphere, all presenting UV and GL emission. Besides the difference in the branch length, also distinct intensity ratios were observed for the used atmospheres. It as seen that the tetrapod nanostructures obtained in air were the ones that depicted stronger green/UV emission ratio, as well as longer branches. On the other hand, the samples produced in humid argon flow displayed UV emission stronger than the visible one. Even so, no clear relation between size and UV/GL intensity ratio could be established.

The premise that the GL was originated from surface-related states was also supported by the findings of Hsu *et al*. [125] regarding polarized luminescence studies from aligned ZnO nanorods. As well, Fabbri *et al.* [126] showed by spatial resolved CL that the GL is mainly localized at grain boundaries of their ZnO nanostructured thin films. Conversely to what was verified for the NBE emission, which did not depend on the size of the nano-grains, the GL intensity varied with the grain, being reduced in grains that exceed 500 nm, suggesting a dominant bulk-like behavior in those cases [126]. In the case of the nanorods, monochromatic CL maps of NBE and GL showed that the NBE emission is mainly originated from the top surface of the hexagonal rod, while the GL signal arises from the lateral nonpolar (1010) surfaces [126]. By the aid of principle simulations of the structural and electronic properties of their defective ZnO systems, the authors conclude that the GL is linked to surface states created by the presence of zinc vacancies, preferentially located at nonpolar (1010) surfaces. Previous spatially resolved PL studies performed by Zhou *et al.* [106] also indicated that the GL displayed by their ZnO micropyramids and ZnO nanorods synthesized by the thermal decomposition was surface-dependent and originated mainly from the defects on/near the surface.

Shalish *et al.* [127] reported the PL analysis on ZnO nanowires grown by chemical vapor deposition on Si (111) wafers and observed that the relative intensity of the NBE emission, regarding the deep level luminescence, is higher for the wires with larger diameters, while the green emission dominated the spectra for the smaller ones. Moreover, this work showed a strong correlation between surface states and the green luminescence, which intensity decreased as the wire dimension increased [127]. By analyzing their results, they concluded that below a certain diameter (~100 nm), the

luminescence properties of their ZnO nanowires was almost exclusively ruled by the properties of the surface, while larger wires (~240 nm) the peak intensity is comparable for both emission and for nanowires with diameters ~540 nm, the NBE is quite stronger that the GL. This result contrast with the ones mentioned above for nanorods produced by Hsu *et at* [123] via a solution-based approach which displayed the yellow band and where the size of the structures did not show any effect on the NBE/visible ratio, pointing once again for the different origins and location of the defects that originate these transitions and that are strongly dependent on the growth procedure.

Paying a closer attention to the UV emission, radiative transitions related to the surface of the structures may also arise in this spectral region. Actually, the group of McGlynn *et al.* [128,129] observed the presence of a high energy excitonic emission at 3.366 eV (at low temperature) in ZnO nanostructures, that was assigned to a surface bound exciton, likely due to an adsorbate, as OH-related species. Moreover, the signal of such recombination was seen to be considerably influenced by the morphology of the nanostructures from which it originates [129].

The effects of the surface recombination, as well as the presence of the depletion region, are not limited to luminescence properties. Actually, it may provide undesirable traps for carriers in several devices, having a profound influence on the electron conduction and carriers mobility properties, which are detrimental for a great number of applications [111,113,127]. Hence, methods that enable an adequate control on the surface properties of the ZnO nanostructures are of substantial importance. For instance, by coating the material or passivating its surface in a way that carrier traps can be blocked or removed should optimize the ZnO emission [130]. On the other hand, surface modification can be used to tailor the optical properties and promote the desired ones [130–134]. In 2015, the surface passivation of ZnO microrods (MRs) produced by LAFD was reported [43]. In that work, it was proved that the 3.31 eV emission line observed in the as-grown MRs (see Figure 7) was related to surface defects and that it could be suppressed by adequate surface plasma passivation treatments. Indeed, this PL feature has been widely reported in the literature and several origins were pointed out, namely the presence of basal plane stacking faults [135–137]. However, the LAFD-produced MRs do not exhibit that type of defects, thus another culprit should be found. On the other hand, Fallert *et al*. [138] analyzed by PL ZnO nanoparticles with diverse diameters and observed that the relative intensity (regarding the D^0X emission) of the strong luminescence band around 3.31 eV increases as the size of the nanoparticles decreases. Taking into account that the 3.31 eV/D^0X intensities ratio is dependent on the surface/volume ratio and proportional to the inverse of the particle size, the authors suggested that this particular luminescence is associated with states present at the surface of the particles, suggesting a bound-exciton-like transition model for the recombination [138]. Moreover, Tainoff *et al.* [139,140] also carried out PL studies on different types of samples (single crystals, nanorods and nanoparticles) and concluded that the 3.31 eV emission is composed by an overlap of different processes, namely a defect-related transition, since the 3.31 eV appeared in the PL spectra of the nanorods even when the FX emission was not observed. The PL studies as a function of the plasma treatment conditions corroborated those claims regarding the correlation between the 3.31 eV and the presence of surface states [43]. As displayed in Figure 7 for the case of the N_2 plasma, which is known to act mostly at the surface due to its limited diffusion in ZnO [141], a complete suppression of this emission was achieved for a plasma treatment at 1000 W, leading to a PL spectral shape resembling the one recorded for the bulk. When the surfaces are passivated, eliminating the species that were present at the surface (*e.g.*

adsorbates), the density of the surface states promoted by them is strongly reduced, together with the decrease/elimination of the depletion region. As so, the bending of the bands can be almost neglected and the bulk recombination processes dominate [43], as exemplified in the right side of Figure 6.

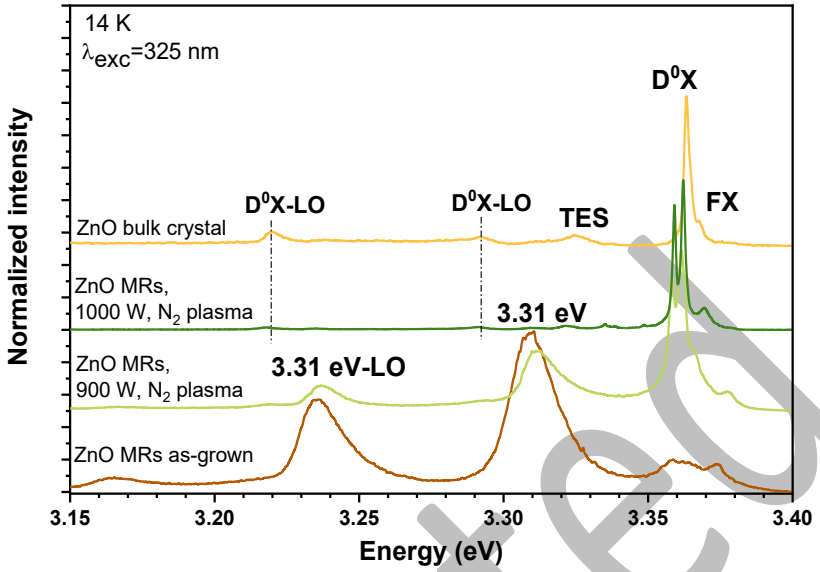

Figure 7 – Low temperature PL spectra obtained for ZnO microrods grown by laser assisted flow deposition and subjected to different N_2 plasma treatments to passivate the surface of the rods. A spectrum of a bulk sample is also displayed for comparison. Data adapted from [43].

For the sake of clarity Table 2 depicts a summary of the above discussed micro and nanostructures, with their correspondent dimensions, growth method and luminescence features.

Table 2 – Summary of the different micro and nanostructures discussed in the text and their correspondent dimensions, growth procedures, post-growth treatments and observed PL features.

Type of structure	Dimensions	Growth procedure	Post-growth treatment	NBE emission	Deep level emission	Observations	References
Nanorods	Diameter <100 nm; lengths of hundreds of nm	Hydrothermal	Annealing at different temperatures (200, 400, and 600 °C) and different atmospheres (air, Ar, N_2, H_2+N_2)	Yes	Yellow to red	• Rods with hexagonal cross-section; • Peak position shifted to higher λ with annealing temperature (in air); • Annealing treatments in air resulted in a prominent red emission; • Annealing significantly enhances the UV emission in all atmospheres except air; • Broad visible band reduced/suppressed with annealing at 600 °C and Ar and N_2 atmospheres and >200 °C for H_2+N_2.	[54,116,120]
Nanorods	2 different diameter range:100–200 nm and 30– 50 nm; length ~500nm	Solution-grown	Annealed in forming gas (H_2+N_2) for 2 h at 450 °C	Yes	Yellow-orange (peak at 600 to 650 nm)	• As-grown samples: NBE intensity much; smaller compared to the defect luminescence; • Annealing in a reducing atmosphere eliminated the yellow-orange luminescence and enhanced the NBE.	[123]
Nano/microrods and microflowers	Diameters from 800 to 400 nm; lengths of tens of μm	Hydrothermal	Differential scanning calorimetric measurements from room temperature to 900 °C	No	Green to red	• Intensity of the PL emission dependent on the ambient and exposure time to laser irradiation; • Almost no NBE emission; • Shift of the peak position of the broad luminescence band to higher energies after thermal analysis.	[23]
Nanorods	Diameter ~50 nm; lengths of hundreds of nm	Vapor phase technique	None	Yes	Green	• NBE/GL ratio dependent on the probed zone of the same rod; • Decreasing of the NBE signal moving from the substrate to the tip; • CL mapping show that GL signal arises from the lateral nonpolar (1010) surfaces.	[115]

Nanowires	Diameters from 50 to ~540 nm; lengths of hundreds of nm	Chemical vapor deposition	None	Yes	Green	• NBE/GL ratio dependent on the diameter of the nanowires; • GL dominates the spectra for smaller nanowires.	[127]
Tetrapods	Branches with lengths ~ 1 µm; needle-like tips	Thermal evaporation of Zn under different conditions	Coating with a surfactant (n-hexyltrichlorosilane)	Yes	Green	• Differences in the ratio of UV and visible emission depending on the growth atmosphere; • Higher NBE intensity for samples grown in humid argon flow; • Tetrapod nanostructures obtained in air showed stronger green; • Addition of a surfactant significantly reduced green emission.	[54,115,118]
Tetrapods	Branches with lengths of hundreds of nm to a few µm; needle-like tips	LAFD	None	Yes	Green to orange	• High NBE/ broad band intensity ratio; • Almost no visible emission at low temperature; • Broad band composed by several emitting centers observed at RT.	[21,142]
Microrods	Diameters from 200 - 500 nm to a few µm; length ~ tens of µm	LAFD	H_2 and N_2 plasma treatment	Yes	Green	• Rods with high aspect ratio hexagonal cross-section; • Intense broad structured band in the green spectral region; • NBE recombination at 14 K dominated by a emission line at ~ 3.31 eV; • 3.31 eV can be reduced and even suppressed with the plasma treatments, particularly with N_2 plasma.	[21,43]

The formation of heterojuncions between ZnO and other materials [7,8,130,142–148], as for instance metal particles, may also have strong effects on the surface recombination processes. For example, the presence of silver particles on the surface of ZnO MRs and tetrapods (TPs) [142] lead to significant changes in the PL outcome of the ZnO micro and nanostructures produced by LAFD (see Figure 8). PL studies performed on the TPs revealed that when the same growth conditions were employed using precursors with and without silver, the resultant samples displayed differences in the energy position of the broad visible bands, as well as in the NBE region. When one compares the spectra obtained for the sample where silver was added, a noticed reduction of the 3.31 eV line relative intensity at 14 K was observed, together with a displacement in the energy peak position of the green broad band (~2.4 eV) against the orange-red (~2.1 eV) spectral region (lower part in Figure 8). One may not be able to clearly identify the defect causing this orange-red emission, but it was observed that it prevails over the green-related one when silver is present. The fact that the green component is suppressed by the metal introduction may also indicate a correlation between this emission and defects located at the surface, as supported by several authors based on evidences of its intensity reduction after surface treatments [54,117]. In fact, a reduction/suppression of the 3.31 eV emission in the samples with silver it was also observed. Since this emission is believed to be also associated with surface states, thus the presence of silver at the ZnO surface may lead to charge transfer from those states to the silver particles, resulting in the photoinduced carriers' partition and hindering the radiative process, which leads to a decrease in the intensity of the mentioned emissions [43].

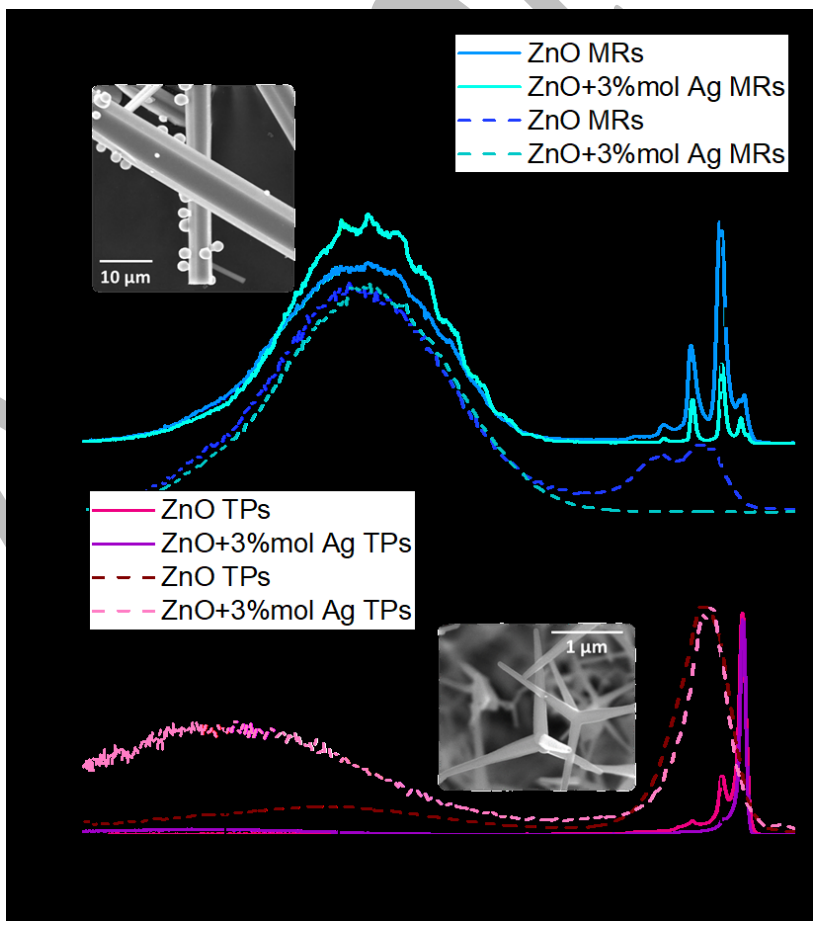

Figure 8 – 14 K and RT PL spectra of ZnO microrods (MRs, top) and tetrapods (TPs, bottom) nominally undoped and grown in the presence of silver (produced by laser-assisted flow deposition). The inset SEM figures show their correspondent morphologies. In the case of the MRs, a sample decorated with silver particles is displayed. Data adapted with permission from WILEY-VCH Verlag GmbH & Co. KGaA [142].

Regarding the MRs (upper part in Figure 8), the differences are not as remarkable as in the case of the TPs' structures. In this case, the structured GL prevails even when Ag was added, with no shift in its peak position, opposed to what was observed for TPs.

In the case of the UV region, and contrarily to the NBE of the TPs, the vibronic assisted 3.31 eV line remained for the samples with silver. However, the relative intensity of this transition when compared with the visible emission was seen to decrease significantly when silver was added, which can again be connected with charge transfer to the metallic particles, preventing recombination, as discussed in the case of the TPs [43]. As these microstructures possess a lower surface-to-volume ratio than the TPs, the fact that the changes in the PL features are less pronounced in this case can be associated with a higher contribution from bulk-related defects and less from the surface-related ones, which have more relevance at the nanoscale. This also suggests that the green bands observed in both structures have different origins. In the case of the microrods bulk defects should be accounted, while for the TPs surface-related states are likely to prevail.

A similar phenomena was found in the case of the ZnO micro and nanostructures produced by flame transport synthesis (FTS) and hybridized with C_{60} molecules [143,149]. The covered of the samples was confirmed both by SEM and Raman analysis, as displayed in Figure 9a and b, respectively. Besides the expected vibrational modes of ZnO described in the Introduction, the samples coated with C_{60} also evidence some of the normal mode frequencies of an isolated C_{60} molecule (labelled with an asterisk) [150]. The spectra were seen to be reproducible when probed in different spots of the same sample, suggesting that the C_{60} coating is fairly homogeneous. For such samples, the green luminescence component of the broad visible band also decreased its contribution with the presence of C_{60} at the surface of the ZnO structures (see Figure 9c). Moreover, this reduction became more accentuated with the increase in the C_{60} content [143]. Such behavior led to the premise that the green luminescence observed in those structures was originated from surface defects and by placing C_{60} molecules at their surface would lead to a passivation of those defects, suppressing the trap-related carriers, and thus reducing the intensity of that green component [143]. Indeed, experimental evidences pointed out to the existence of charge transfer processes between ZnO and C_{60}, both from C_{60} to ZnO, as well as in the opposite direction, simultaneously. Likewise, the amount of carriers that populate the excited states of the green luminescence center(s) is reduced and a quenching of its intensity is observed [143,149].

Besides the effect on the broad visible band, the coverage of the ZnO surface with the carbon species also led to variations in the NBE region. Conversely to what was verified for the green emission, the relative intensity of the NBE increases with the amount of C_{60} at the ZnO surface for both rods and tetrapods [143,149]. In fact, the intensity of this emission for the as-grown samples was almost negligible when compared to the visible one. However, by adding the C_{60} molecules, the NBE becomes the dominant emission at low temperature (Figure 9d). This phenomenon was tentatively assigned to the presence of a higher concentration of electron-hole pairs in the semiconductor surface, promoted by the contact with the C_{60} molecules, which resulted in an enhancement of the excitonic and surface related transitions, supporting previous studies in other ZnO/carbon composites [144,149], and corroborating the existence of charge transfer from C_{60} to the semiconductor surface, as discussed above [143,149].

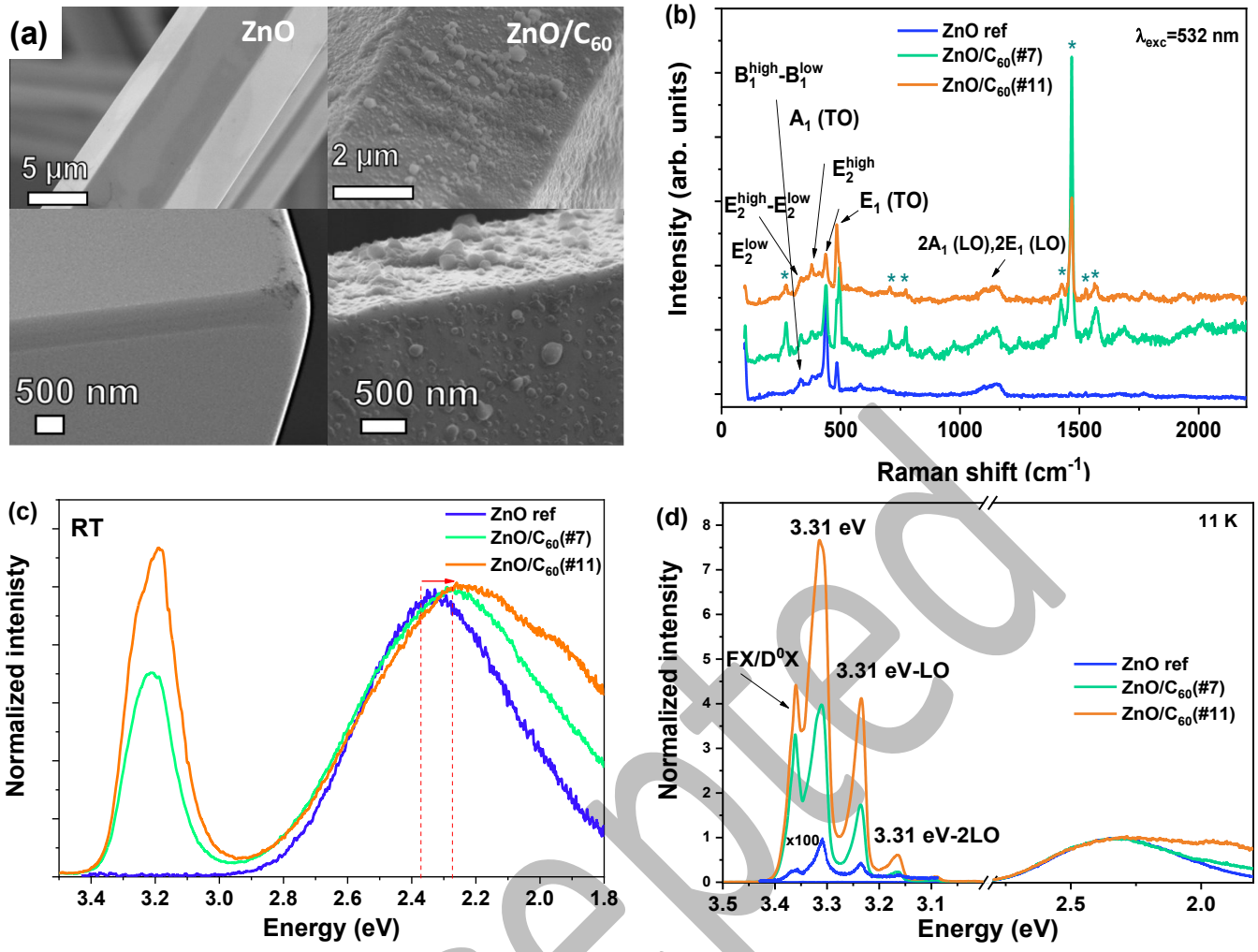

Figure 9 – (a) SEM picture with an example of the ZnO microrods prepared by FTS before (left) and after (right) C_{60} coverage on the ZnO microrods prepared by FTS (7 flooding). (b) RT Raman spectra ZnO/C_{60} composites with different C_{60} content, obtained in backscattering configuration and under 532 nm laser excitation. The asterisks denote the modes associated with C_{60}. (c) RT and (d) 11 K PL for the ZnO and ZnO/C_{60} microrod samples with different C_{60} content (7 and 11 floodings). The PL spectra were obtained with the 325 nm He-Cd laser line and normalized to the broad emission maxima. The data was adapted with permission from reference [149].

In addition to C_{60}, ZnO nanostructures have been used to form composites with different carbon-based materials, as carbon nanotubes (CNTs) [144,145,151], activated carbon [152], laser-induced graphene [153], and so on. As an example, Rodrigues *et al* [145] showed that the overall intensity of the PL signal was enhanced by placing the ZnO structures on top of an array of vertically-aligned CNTs, while maintaining the same spectral shape. Such enhancement was attributed to an increase in the concentration of the carriers at the surface of the ZnO nanostructures promoted by their contact with the CNTs. On the other hand, when similar ZnO nanostructures were mixed with functionalized CNTs to form a flexible membrane called buckypaper [144], the spectral shape of the PL signal was seen to change, namely evidencing an increase in the relative intensity of the 3.31 eV line mentioned above. In this case, it was observed that the formed membranes exhibited the strong luminescence inherent to the ZnO structures, combined with the excellent electrical conductivity properties associated with the CNTs. Nevertheless, it is important to bear in mind that the luminescence behavior of the ZnO

structures when forming composites with the different carbon allotropes may differ from sample to sample, depending on the type of interaction that is established between the two materials and the subsequent alignment of the energy levels, namely the defect-related ones [143].

Coating ZnO with materials with a larger bandgap and with an higher conduction band edge than that of ZnO have also showed interesting results [130,131,154,155]. For instance, Li *et al.* [155] achieved a great enhancement of the NBE emission of ZnO nanorods, together with a substantial reduction of the defect-related one, by coating the ZnO surface with SnO nanoparticles, forming ZnO/SnO nanocomposites. Additionally, Chen *et al.* [131] also observed that Al_2O_3 coating on ZnO nanorods resulted in the suppression of the deep level emission, which was attributed to the passivation of the surface-related defects, leading to a flat-band effect that promotes the NBE recombination in detriment of the surface-related one. Such findings also indicate that the surface states of the as-grown ZnO nanorod are in the origin of the deep level emissions [131]. The formation of composites/hybrid networks of ZnO tetrapodal structures produced by FTS and mixed with different metal oxide compounds, Me_xO_y and $Zn_xMe_{1-x}O_y$ with Me = Fe, Cu, Al, Sn, Bi [7,8] (see Figure 10), was also studied, revealing interesting results. Such materials were prepared by mixing the as-grown tetrapods with different metals, at different weight ratios, followed by subsequent thermal annealing. Depending on the metal oxide used as precursor, different features were obtained. Figure 10 a to c show examples of the microstructures formed in the presence of Fe, Cu and Sn, respectively.

In the case of the ZnO−Fe_2O_3 hybrid structures, Fe_2O_3 particles appear randomly distributed on the surface of the ZnO tetrapods through the entire network of tetrapods (Figure 10a). On the other hand, ZnO-CuO samples exhibit an alloy-melt-like microstructures instead of forming the nano/microparticles (Figure 10b), as in the previous case. By hybridizing the samples with SnO_2, besides the presence of the ZnO tetrapods, the formation of additional microparticles' agglomerates randomly distributed through the network could also be identified (Figure 10c). In this case, those particles were seen to correspond to a Zn_2SnO_4 phase, as corroborated by Raman analysis (Figure 10d). Probing the sample in different regions revealed that besides the ZnO wurtzite crystalline phase always present, an additional zinc stannate cubic-faced-centred spinel structure was detected in a heterogeneously distribution, as was observed in SEM. This phase was clearly identified in the Raman spectra of Figure 10d, where two additional well-defined peaks were identified at 535 and 668 cm^{-1}. Regarding the PL features of these different composites/hybrid structures (Figure 10e), it was shown that the PL outcome could be tuned depending on the compound used to form hybrid ceramic networks with ZnO, as illustrated by the shift in the peak position of the broad visible band depending on the additional metal oxide present. Moreover, in the case of the sample with Al, the peak position and spectra shape of the defect related emission was dependent on the probed region of the sample, pointing to an inhomogeneous distribution of the additional metal oxide phase, as also identified by the Raman analysis for the sample with Sn [7,8].

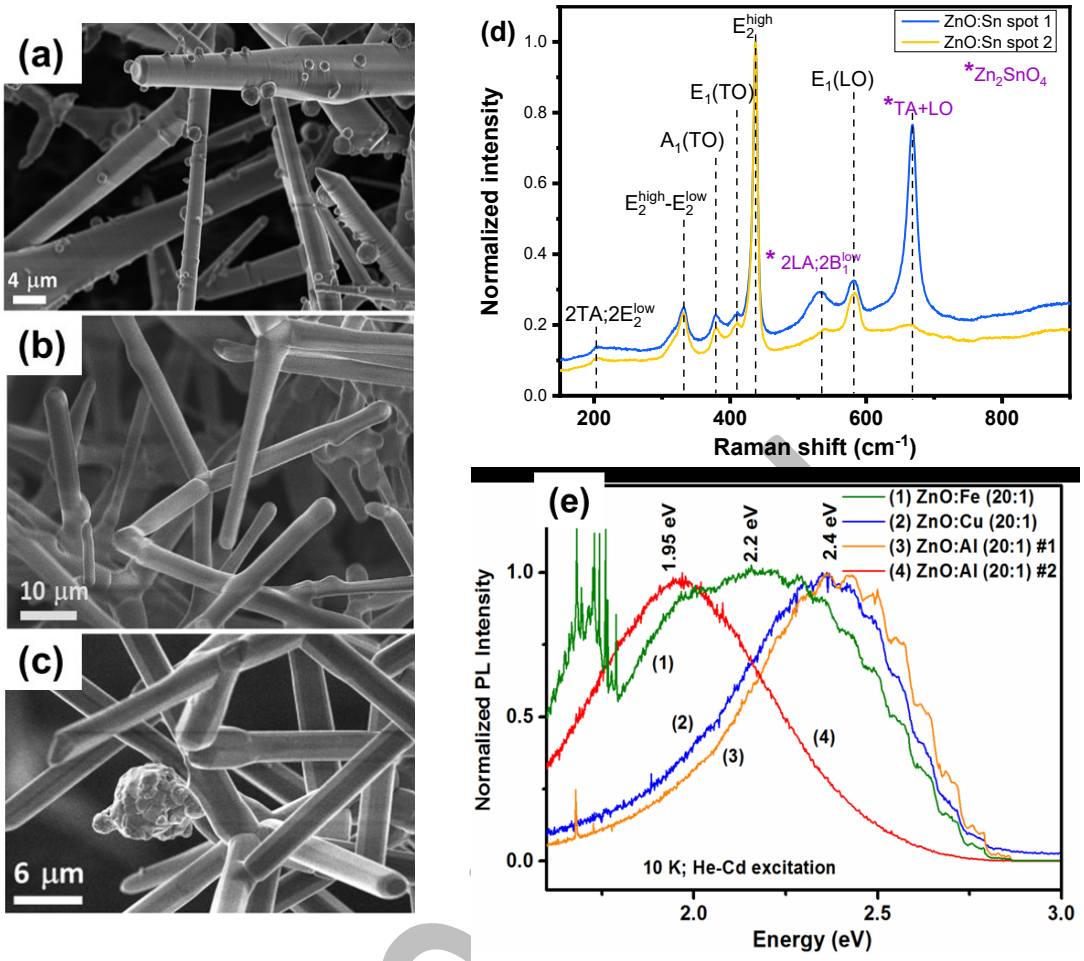

Figure 10 –Representative SEM images of the same samples produced by FTS and hybridized with different metal oxides (a) ZnO:Fe, (b) ZnO:Cu and (c) ZnO:Sn. (d) Raman spectra for the sample produced with Sn, evidencing the presence of an Zn_2SnO_4 phase. (e) Normalized 10 K PL of the composite samples hybridized with different metal oxides, excited with 3.8 eV photon energy, (1) ZnO-T:Fe (weight ratio of 20:1); (2) ZnOT:Cu (20:1); and (3,4) ZnO-T:Al (20:1) in different regions of the sample. Data reprinted with permission from [7,8].

3. Applications

ZnO has been used in an uncountable number of applications, ranging from optoelectronics, sensing, photovoltaics, photocatalysis, biomedical engineering, among others [3,6–8,50,51,142,156–168]. Perhaps one of the most well-known application of ZnO is as transparent conductive oxide (TCO) for light emitting diodes (LEDs), solar cells and transparent electronics, among others. For such purposes, high transparency and high electrical conductivity are required properties [169], which can be fulfilled by doped ZnO thin films. The Zn abundance and the low cost production of ZnO, associated to its low toxicity and high stability against the H plasma exposure [170], makes doped ZnO thin films serious candidates to replace conventional TCOs based on tin doped indium oxide (ITO) and fluorine-doped tin oxide (FTO) [169]. As In is a rare material, Zn is seen as a viable alternative to produce the metal-oxide based TCOs that are demanded by the growing devices market. The *n*-type high conductivity can be easily reached in ZnO by an appropriate controlled *in-situ* or *ex-situ* doping, employing shallow donor impurities as for instance hydrogen or group III elements (*e.g.,* Al, Ga and In) [58,169,171–174]. Among the most studied dopants, Al is known to increase the optical transparence region

for heavily doped material due to the Burstein-Moss and bandgap renormalization effects [175–178]. Moreover, the material exhibits low electrical resistivity values ($ca.\ 10^{-4}\Omega.cm$) similar to the ones measured for ITO [179]. A current status of ZnO as TCO was recently reported by Mallick *et al.* [169] and Coll *et al.* [180].

Despite the fact that ZnO was considered as a potential candidate for the production of blue or UV LEDs, the lack of reliable *p*-type conductivity hinders the achievement of ZnO based homojunction for such devices. However, several attempts have been essayed to obtain *p–n* heterostructures with *n*-type ZnO/*p*-type semiconductors, such as Si, GaN, AlGaN, SiC, GaAs, etc., while still using ZnO as the active layer [2,181]. More than a decade ago, Look and co-authors [182] reported a compilation of several light emitting devices based on ZnO, foreseeing good prospects for its application in the lighting industry. Though, the mismatch between the lattice parameters has limited the growth of heterostructures free of defects, even when materials with similar lattice parameters are used, as is the case of *p*-GaN and 4H *p*-SiC [181]. Thus, there are still a number of important issues that need to be addressed, which require further investigation before ZnO can be used in commercial competitive applications in the lighting field. Nevertheless, some noteworthy results were reported for *n*-type ZnO/*p*-type GaN heterojunctions, which possess similar direct bandgap and exhibit only a 1.8 % of lattice mismatch [183]. Rogers *et al*. [184–188] have made interesting progresses in the development of such devices. For instance, they reported the production of *n*-ZnO/*p*-GaN:Mg heterojunctions grown on *c*-Al_2O_3 substrates [184,185] via combined pulsed laser deposition and metal organic chemical vapor deposition for the growth of ZnO and GaN:Mg, respectively. The devices exhibited an intense PL emission peaked at 375 nm and an almost negligible green emission, indicating a low density of defects present in the ZnO structures [184]. The high crystalline quality, as well as the good surface/interface morphology, were further corroborated by X-ray diffraction, SEM and atomic force microscopy (AFM) studies [184,185]. The emission at 375 nm was also clearly identified by RT electroluminescence (EL). A comparison of the RT EL and PL spectra pointed to the association between the observed emission and excitonic recombination occurring in the ZnO layer. Such results evidenced the possibility of accomplish significant hole injection from the GaN:Mg into intrinsically doped ZnO, thus highlighting the potential of the *n*-ZnO/*p*-GaN:Mg heterostructures as UV LEDs based on the excitonic emission from ZnO [184]. Another UV LED peaked at ~389 nm based on a *n*-ZnO/*p*-AlGaN heterojunction deposited on 6H-SiC substrates was reported by Alivov *et al.* [189]. In this case, the ZnO layer was produced by chemical vapor deposition and the *p*-type AlGaN was grown by hydride vapor phase epitaxy. The strong UV emission was associated to recombination within the ZnO layer and it was observed when applying a forward bias to the device, being stable up to 500 K. In 2014, Schuster *et al.* [190] published a work where simulations of the electronic band structure of a *p*-GaN/*n*-ZnO heterointerface were conducted. They conclude that the interface between the two materials reveals various possibilities of band structure alignment, depending on the polarity and strain of both wurtzite materials. Therefore, a profound knowledge of the band alignments is extremely important to design the envisaged applications. Moreover, spontaneous polarization was also seen to induce additional effects on the band structure and the location of the recombination region. Besides the theoretical simulations, these authors also fabricated *p*-GaN/*n*-ZnO heterojunctions in the form of nanowires (*p*-GaN nanowires capped by *n*-ZnO) by plasma-assisted molecular beam epitaxy (PAMBE) [190]. Optical studies on those wires revealed that the emission was mainly dominated by ZnO-related recombination in the UV spectral region (~3.26 eV), showing a strong stimulated emission with a low threshold (> 55 kW/cm^2), confirming the high interest of this type of

heterojunctions in the production of high efficient LEDs and laser diodes emitting in the UV spectral range [190].

Photocatalysis has also been a very active field for ZnO [142,156,158,191–195]. In fact, ZnO is one of the most studied semiconductors in this area [191,196–198], right after titanium dioxide (TiO_2). Even though ZnO has inferior chemical stability when compared to TiO_2, this semiconductor possesses a high photosensitivity, surface reactivity and the ability to be easily produced in a wider range of morphologies, enabling the maximization of its surface area. The latter is crucial for photocatalytic applications, since the reaction will occur at the surface of the semiconductor [142,192,199–202]. For instance, for tetrapods and microrods produced by the LAFD technique [142] and applied as photocatalysts in the degradation of the methylene blue (MB) dye, the nano tetrapods were found to exhibit the fastest degradation time, indicating that the photocatalytic activity is strongly dependent on the morphology [140]. The results allowed to conclude that the higher surface-to-volume ratio provided by the nanometric dimensions, as well as the shape of the tetrapod structures and their low tendency to aggregate, supported a higher area for the photocatalytic reactions to occur. Moreover, these samples also exhibited a higher concentration of surface related defects, which may contribute to the mediation of the photocatalytic reaction, highlighting once again the importance of surface defects in ZnO-based applications. Additionally, an evaluation on the influence of the presence of silver in those samples revealed that degradation time was decreased in both structures due to a higher efficient charge separation promoted by the metal particles on the surface of the semiconductor [142]. Guo *et al* [192] also conducted a work where the photocatalytic performance of different ZnO nanostructures was compared, namely tetrapods, commercial nanoparticles and powders. Tetrapods revealed the highest photocatalytic activity of all the morphologies analyzed and for all the dyes investigated, despite having a lower surface area when compared to the nanoparticles due to different surface properties/defects in the different structures. Furthermore, the orientation of the ZnO surfaces may also play an important role in both efficiency, stability and photocatalytical activity [192]. Another conclusion from the work of Guo *et al.* [192] is that the native defects are a decisive factor in the photocatalytic efficiency. Still, the role on these defects is not completely known yet, since native defects also contribute to enhance the carriers' separation and serve as active centers on the photocatalyst surface, which will have positive effects on photocatalytic efficiency [203]. In this sense, defect engineering arises as an interesting tool to manipulate the native defect properties in order to improve the photocatalytic response [203]. As an example, we would like to mention the work of Liu *et al* [204] where ZnO tetrapods were exposed to plasma treatments with different gases promoting distinct types of defects on the surface of the ZnO tetrapods. In fact, different PL features were also identified after these treatments and X-ray photoemission spectroscopy (XPS) put in evidence the formation of a higher amount of oxygen deficiencies after plasma treatments with argon and hydrogen. A clear connection between the photocatalytic activities and the surface composition measured by XPS was found. A higher concentration of oxygen-related defects, as well as lightly bound oxygen and hydroxyl species near the surface of ZnO were seen to lead to lower catalytic performance, which is opposed to what is typically reported for this material [204]. The best photocatalytic activity was displayed by the sample treated in an oxygen plasma [204]. Besides defect manipulation, the formation of heterostructures and composite materials have also been pointed out as a potential way to improve the photocatalytic properties of ZnO [142,205,206]. By forming heterostructures with adequate band alignment it is possible to induce charge separation with advantages for the efficiency of the photocatalytic effect [203]. In fact, this was what was demonstrated by the decorated

LAFD ZnO structures with silver particles [142], as described above. Recently, Park *et al.* [207] also showed the improvement of the photocatalytic action using 3D hybrid composites based on carbon nano-onion (CNO)-functionalized zinc-oxide tetrapods (T-ZnO-CNO 3D). The authors assessed the performance of such structures in the degradation of 2,4-dinitrophenol (DNP) and observed that the photodegradation efficiency of the T-ZnO-CNO hybrid composite was enhanced by ~92% when compared to that of the CNOs and ZnO tetrapods. [207].

The use of ZnO nanostructures in the fabrication of photovoltaic solar cells have also aroused the interest of the research community. Djurišic *et al.* [157] provide an overview of the possible applications of ZnO-based materials in solar cells, emphasizing the use of ZnO for contacts and/or light trapping, as a part of polymer-based solar cells, as *n*-type material in heterojunction solar cells with other inorganic materials and, of course, in dye-sensitized solar cells (DSSCs). The latter is probably one of the most explored application of ZnO in this field. The interest in this type of photovoltaic cells arose from their low cost and reasonably high light-to-electricity conversion efficiency [208], as well as innovative design opportunities, such as transparency and multicolor options, flexibility and lightweight [209]. Although this field is largely dominated by TiO_2, ZnO was one of the first semiconductor materials to be used in sensitization studies and present several interesting properties, as the similar bandgap and electronic affinities, that (in theory) make it an alternative to TiO_2 [52,210–213]. However, despite the great amount of work conducted in this area a few years ago [48–50,52,53,157,208], the energy conversion efficiency of ZnO based DSSCs remains lower than the values found for TiO_2. Among other factors, its poor chemically stability under acidic dye solutions has been pointed as one of the major problems [212,213]. In 2012, Anta *et al.* [212] revised the status of the ZnO-based DSSCs up to that point and suggested that the recurrent low performance of this material when compared to TiO_2 could be related to the lack of efficient dyes that do not deteriorate the ZnO surface, as well as the presence of a myriad of surface-related states that have an important impact in the efficient charge-separation across the surface of the semiconductor. Therefore, surface control seems to be a mandatory aspect for reliable and competitive DSSCs fabrication. Notwithstanding, some interesting works were reported in the last decades regarding the contribution of ZnO in different types of photovoltaic devices. For instance, in 2016, the application of a combination of ZnO nanoparticles and tetrapods grown by LAFD as photoelectrode in DSSCs was reported [50], showing an efficiency of ~3% achieved under simulated AM 1.5 illumination conditions for a dye (N719, Ru-based) loading time of 1 h, which is an efficiency value comparable to what has been typically identified in ZnO [214]. Recently, Mohamed *et al.* [215] fabricated a DSSC using nanocomposites of ZnO nanorods incorporated into a carbon nanotube-graphene oxide (ZnO/CNT-GO) structure and sensitized also with the N719 dye. A power conversion efficiency of 7.73% was achieved for this structure, which is one of the best values reported until now for a ZnO-based DSSC.

Structures with a high surface-to-volume ratio, as is the case of the mentioned tetrapods, have also triggered immense attention in the sensing field [7,8,216,217], since their morphology allows ease accessibility to the surface of their arms, as their geometry promotes the formation of an interconnected highly porous network [51]. In the case of gas sensing devices, for instance, this type of structure allows an easy diffusion of gas molecules along the arms of the TPs [7,8]. In 2005, Xiangfeng *et al.* [217] reported the fabrication of gas-sensors based on ZnO nanotetrapods prepared by evaporation of pure Zn in different gas flows, humidified Ar, dry Ar, humidified N_2 and dry N_2. The growth in different atmospheres let to variation in arm lengths and diameters. Such differences

conducted to distinct gas-sensor responses. The best result was accomplished for the sensors prepared with tetrapods produced in humidified Ar atmosphere, evidencing a high response to dilute C_2H_5OH, with good selectivity and short response time [217]. Calestani *et al.* [216] also used ZnO tetrapods produced from a vapor phase growth process to fabricate gas sensing devices to probe different gases, CH_3CH_2OH, NO_2, CO and H_2S. The best response was obtained for H_2S, with response values of sensitivity ~25 and ~100 at 1 ppm and 5 ppm, respectively. Moreover, the other tested gases also displayed good results, with the exception of CO. Sensitivity values of ~20 for 20 ppm of NO_2 and 50 ppm of CH_3CH_2OH were recorded, while a value lower than 0.2 towards 10 ppm of CO was measured. The group of Mishra *et al.* [7,8,22,51,149,151,165] have also devoted great attention to the research of ZnO-based tetrapodal networks for gas sensing applications. By forming composites with other metal oxides or carbon materials, it is possible to tune not only the luminescence, as described above, but also their gas sensing properties [7,8]. The studies revealed improved performance of the hybrid networks when compared with the ones composed only by pure ZnO tetrapods. Moreover, the gas sensing studies highlighted the possibility to control and change/tune the selectivity of the materials, depending on the element content ratio and the type of added metal oxide in the ZnO hybrid networks. For instance, adding bismuth to the ZnO network promotes the detection of hydrogen, while different tin contents results in different selectivity towards carbon monoxide [7]. This sensitivity enhancement is mainly associated with additional modulation of the electrical resistance by the built-in potential barriers between the formed heterojunctions during adsorption and desorption of gaseous species, while the selectivity tuning to different gases is attributed to the catalytic properties of the metal oxides after hybridization [7,8]. In the case of the $ZnAl_2O_4$-surface functionalized ZnO structures [165], an improved response to H_2 was verified when compared to pristine ZnO-T networks. Both microrod and tetrapod morphologies were tested and even thought all devices showed an excellent selectivity to the probed gas, the tetrapod-based ones demonstrated higher performance. Devices based on ZnO tetrapods coated with C_{60} molecules were also prepared [149] and tested for different volatile compounds (concentration 100 ppm), namely ethanol, n-butanol, isopropanol and acetone, as well as H_2 (concentration 1000 ppm). The best response was achieved for ethanol detection in all the tested devices operating at RT. By increasing the amount of C_{60} the gas response to ethanol vapors was enhanced [149].

Besides gas sensing, ZnO is also employed in the development of biosensors. According to IUPAC (International Union of Pure and Applied Chemistry), a biosensor is a device that uses a biological recognition element (enzymes, antibodies, aptamers, etc.) to provide specific quantitative or semi-quantitative analytical information regarding the detection of the analyte [218]. This bioreceptor is in direct spatial contact with the transducer element and when the reaction with a target species occurs, this biologic interaction is converted by the transducer into a physical signal [159,218]. Therefore, the transducer is one of the key elements of a biosensor and defines the methodology for the sensing measurements [159]. ZnO has been used as transducer platform in different types of sensors [159,219–224]. The ability to produce ZnO nanostructures with various sizes, shapes and properties has a profound influence on the immobilization of biomolecules [159]. Moreover, its biochemical stability and biocompatibility [225,226], and high isoelectric point (IEP~ 9.5) suitable for the immobilization of low IEP proteins [222,225–229] constitute important properties for biosensing. The most common sensing platforms are based on electrochemical measurements [222,226,229,230], as the biosensors reported by Shanmugam *et al.* [229]. In this case, vertically oriented ZnO nanostructures where used as transducers for detection and quantification of cardiac troponin-T from

human serum. Anti-troponin-T antibodies were used as bioreceptors and the surface of the transducer was further passivated with a protein-free blocking buffer (Superblock) to avoid non-specific interaction between the analyte and the ZnO surface. Aliquots of solutions containing different concentration of cardiac troponin-T were added to the surface of the sensor (starting with lowest concentration) and left to incubate during 20 min. Their results showed the tuning of the electrical response of the sensor with the different analyte concentrations, allowing to define a calibration curve for the device as a function of the troponin-T dose. A detection limit of 0.1 pg/ml was achieved using a combination of AC and DC spectroscopies techniques. In 2016, Tereshchenko *et al.* [159] published a review paper on optical biosensors based on ZnO nanostructures. Indeed, owning to their excellent optical properties, ZnO appears as an excellent candidate to be used as transducer element in optical-based sensors. These authors provided an overview of the main functionalization approaches employed on ZnO nanostructures to immobilize the bioreceptor on its surface, as well as on the different types of optical signals that can be used for analyte detection, namely surface plasmon resonance (SPR), ellipsometry, reflectometry, interferometry, surface enhanced Raman scattering (SERS) or photoluminescence [159]. SPR and SERS-based sensors dominate the optical sensing field, but PL-based sensing has been arising as an alternative since it is a simple and exceptionally sensitive method for characterizing the surface of the samples, especially surface defects and the nanobiointerface [159]. A luminescence-based sensor for *Salmonella* detection was accomplished by Viter *et al.* [223] using ZnO nanorods. The biorecognition layer was prepared by immobilization of anti-*Salmonella* antibodies on the surface of nanorods, which resulted in an intensity increase of ZnO PL features. After further reaction with *Salmonella* antigens, the PL intensity decreased proportionally to antigen concentrations in the range of 10^2 – 10^6 cell/ml [223]. In 2018, Ghosh *et al.* [231] used Al-doped ZnO thin films for the fabrication of a glucose sensor using the glucose oxidase enzyme as biorecognition element. The detection was based on the quenching of the luminescence signal with increasing glucose concentration and a sensitivity of 20 μM was obtained [231]. The quenching of the PL intensity was explained by the formation of H_2O_2 as a sub-product of glucose degradation through the enzyme action. It was proposed that the presence of H_2O_2 promotes electron transfer from the ZnO to the H_2O_2 molecules, leading to a decrease in the radiative recombination at the surface states involved [225,231]. This effect was also reported by Sarangi *et al.* [225]. They used high-quality ZnO nanorods grown on GaN substrates by the hydrothermal method and relied on the direct oxidation of the glucose molecules via a photocatalytic effect promoted by the ZnO rods. A strong decrease in the PL intensity of the NBE recombination was verified with the increased glucose concentrations, and the calibration curve exhibited a good linearity, with a sensitivity of 1.4%/mM over the 0.5–30 mM range. Furthermore, interfering species as bovine serum albumin, ascorbic acid and uric acid were also tested and the sensors revealed a good selectivity for glucose. In fact, real human serum samples were probed and the results match well the ones obtained by the standard clinical method, confirming the good reliability of those sensors [225].

Much more examples could be given regarding the applications of this well-known semiconductor, since its properties are exceptionally appealing for device industry, especially at the nanoscale. Thus, the research on ZnO nanostructures remains a hot topic in the scientific community.

4. Concluding remarks

In this manuscript, we presented a broad review of the photoluminescence properties of bulk and ZnO micro/nanostructures. The discussion starts from the fundamental properties of ZnO, to the different radiative recombination processes widely discussed in the literature and includes some examples of the vast range of applications where this semiconductor has been employed. We intended to shown that even though the luminescence properties of bulk ZnO are commonly known from several decades, some open points remain to be addressed. By reducing the crystal dimensions to the nanoscale, the surface phenomena are seen to frequently prevail over the bulk. As the surface-to-volume ratio for the nanostructures is high, the surface characteristics will have a profound influence on the properties of the material, namely the optical ones. Indeed, the surface can be seen as a kind of defect introduced by the presence of dangling bonds on surface atoms that can easily adsorbe additional atoms/molecules, altering the surface charge density that subsequently induces the formation of a depletion region at the surface of the material. Likewise, the distribution of the surface *vs* the bulk defects will play a key role in tailoring the properties of the ZnO and consequently on the devices' performance. Certainly, the existence of surface-related defects, which are strongly dependent on the growth methods, brought further complexity to the discussion on the chemical origin of the different luminescence features identified for ZnO. The major theories accepted nowadays for the origin of the numerous defect-emitting centers were presented in this paper in order to comprehensively compile the countless information that can be found in the literature. On the other hand, the use of optical spectroscopic techniques were found to be powerful practices to the identification of optically active defects and surface-mediated properties that account for the physical explanation of a given material-related application, namely in electronics, optoelectronics and sensing.

Author Contributions

The manuscript was written through contributions of all authors. All authors have given approval to the final version of the manuscript

Acknowledgments

This work was financially supported by FEDER funds through the COMPETE 2020 Programme and National Funds through FCT - Portuguese Foundation for Science and Technology under projects UID/CTM/50025/2019 and POCI-01-0145-FEDER-028755. Acknowledgments are also due to Professor F. M. Costa from the University of Aveiro and to Professor Y. K. Mishra from the University of Kiel for supplying ZnO micro and nanostructures, grown by LAFD and FTS respectively.

Declarations of interest: none

Data Availability

The processed data required to reproduce these findings can be provided upon request.

References

[1] C. Jagadish, S. Pearton, Zinc Oxide Bulk, Thin Films and Nanostructures, Elsevier, 2006. doi:10.1016/B978-0-08-044722-3.X5000-3.

[2] U. Özgür, Y.I. Alivov, C. Liu, A. Teke, M.A. Reshchikov, S. Doğan, V. Avrutin, S.-J. Cho, H. Morkoç, A comprehensive review of ZnO materials and devices, J. Appl. Phys. 98 (2005) 041301. doi:10.1063/1.1992666.

[3] C. Klingshirn, ZnO: From basics towards applications, Phys. Status Solidi. 244 (2007) 3027–3073. doi:10.1002/pssb.200743072.

[4] Z.C. Feng, ed., Handbook of Zinc Oxide and Related Materials: Volume Two, Devices and Nano-Engineering, CRC Press, 2012.

[5] C.F. Klingshirn, A. Waag, A. Hoffmann, J. Geurts, Zinc Oxide: From Fundamental Properties Towards Novel Applications, 1st ed., Springer, 2010.

[6] S.C. Singh, Zinc Oxide Nanostructures; Synthesis, Characterizations and Device Applications, J. Nanoeng. Nanomanufacturing. 3 (2013) 283–310. doi:10.1166/jnan.2013.1147.

[7] V. Postica, J. Gröttrup, R. Adelung, O. Lupan, A.K. Mishra, N.H. de Leeuw, N. Ababii, J.F.C. Carreira, J. Rodrigues, N. Ben Sedrine, M.R. Correia, T. Monteiro, V. Sontea, Y.K. Mishra, Multifunctional Materials: A Case Study of the Effects of Metal Doping on ZnO Tetrapods with Bismuth and Tin Oxides, Adv. Funct. Mater. 27 (2017) 1604676. doi:10.1002/adfm.201604676.

[8] O. Lupan, V. Postica, J. Gröttrup, A.K. Mishra, N.H. de Leeuw, J.F.C. Carreira, J. Rodrigues, N. Ben Sedrine, M.R. Correia, T. Monteiro, V. Cretu, I. Tiginyanu, D. Smazna, Y.K. Mishra, R. Adelung, Hybridization of Zinc Oxide Tetrapods for Selective Gas Sensing Applications, ACS Appl. Mater. Interfaces. 9 (2017) 4084–4099. doi:10.1021/acsami.6b11337.

[9] G. Lu, J. Xu, J. Sun, Y. Yu, Y. Zhang, F. Liu, UV-enhanced room temperature NO2 sensor using ZnO nanorods modified with SnO2 nanoparticles, Sensors Actuators, B Chem. 162 (2012) 82–88. doi:10.1016/j.snb.2011.12.039.

[10] E. Comini, G. Faglia, M. Ferroni, G. Sberveglieri, Gas sensing properties of zinc oxide nanostructures prepared by thermal evaporation, Appl. Phys. A. 88 (2007) 45–48. doi:10.1007/s00339-007-3978-9.

[11] X. Wang, J. Zhou, J. Song, J. Liu, N. Xu, Z.L. Wang, Piezoelectric Field Effect Transistor and Nanoforce Sensor Based on a Single ZnO Nanowire, Nano Lett. 6 (2006) 2768–2772.

[12] B. Kumar, S.-W. Kim, Energy Harvesting Based on Semiconducting Piezoelectric ZnO Nanostructures, Nano Energy. 1 (2012) 342–355.

[13] D. Sharma, J. Rajput, B.S. Kaith, M. Kaur, S. Sharma, Synthesis of ZnO Nanoparticles and Study of Their Antibacterial and Antifungal Properties, Thin Solid Films. 519 (2010) 1224–1229.

[14] J.S. Tawale, K.K. Dey, R. Pasricha, K.N. Sood, A.K. Srivastava, Synthesis and characterization of ZnO tetrapods for optical and antibacterial applications, Thin Solid Films. 519 (2010) 1244–1247. doi:10.1016/j.tsf.2010.08.077.

[15] R. Wahab, Y.-S. Kim, A. Mishra, S.-I. Yun, H.-S. Shin, Formation of ZnO Micro-Flowers Prepared via Solution Process and Their Antibacterial Activity, Nanoscale Res. Lett. 5 (2010) 1675.

[16] U. Özgür, D. Hofstetter, H. Morkoç, ZnO Devices and Applications: A Review of Current Status and Future Prospects, Proc. IEEE. 98 (2010) 1255–1268. doi:10.1109/JPROC.2010.2044550.

[17] E.M.C. Fortunato, P.M.C. Barquinha, A.C.M.B.G. Pimentel, A.M.F. Gonçalves, A.J.S. Marques, R.F.P. Martins, L.M.N. Pereira, Wide-bandgap high-mobility ZnO thin-film transistors produced at room temperature, Appl. Phys. Lett. 85 (2004) 2541. doi:10.1063/1.1790587.

[18] S. Masuda, K. Kitamura, Y. Okumura, S. Miyatake, H. Tabata, T. Kawai, Transparent thin film transistors using ZnO as an active channel layer and their electrical properties, J. Appl. Phys. 93 (2003) 1624. doi:10.1063/1.1534627.

[19] D.C. Look, Recent advances in ZnO materials and devices, Mater. Sci. Eng. B. 80 (2001) 383–387. doi:10.1016/S0921-5107(00)00604-8.

[20] L. Schmidt-Mende, J.L. MacManus-Driscoll, ZnO - nanostructures, defects, and devices, Mater. Today. 10 (2007) 40–48. doi:10.1016/S1369-7021(07)70078-0.

[21] J. Rodrigues, A.J.S. Fernandes, T. Monteiro, F.M. Costa, A review on the laser-assisted flow deposition method: growth of ZnO micro and nanostructures, CrystEngComm. 21 (2019) 1071–1090. doi:10.1039/c8ce01773e.

[22] Y.K. Mishra, G. Modi, V. Cretu, V. Postica, O. Lupan, T. Reimer, I. Paulowicz, V. Hrkac, W. Benecke, L. Kienle, R. Adelung, Direct Growth of Freestanding ZnO Tetrapod Networks for Multifunctional Applications in Photocatalysis, UV Photodetection, and Gas Sensing, ACS Appl. Mater. Interfaces. 7 (2015) 14303–14316. doi:10.1021/acsami.5b02816.

[23] A. Pimentel, D. Nunes, P. Duarte, J. Rodrigues, F.M. Costa, T. Monteiro, R. Martins, E. Fortunato, Synthesis of Long ZnO Nanorods under Microwave Irradiation or Conventional Heating, J. Phys. Chem. C. 118 (2014) 14629–14639. doi:10.1021/jp5027509.

[24] D.C. Reynolds, D.C. Look, B. Jogai, Fine structure on the green band in ZnO, J. Appl. Phys. 89 (2001) 6189–6191. doi:https://doi.org/10.1063/1.1356432.

[25] H. Morkoç, Ü. Özgür, Zinc Oxide: Fundamentals, Materials and Device Technology, John Wiley & Sons, 2008.

[26] S.M. Sze, Physics of Semiconductor Devices, Wiley, 1981.

[27] M.R. Wagner, J.-H. Schulze, R. Kirste, M. Cobet, A. Hoffmann, A. V. Rodina, B.K. Meyer, U. Röder, K. Thonke, Γ_{7} valence band symmetry related hole fine splitting of bound excitons in ZnO observed in magneto-optical studies, Phys. Rev. B. 80 (2009) 205203. doi:10.1103/PhysRevB.80.205203.

[28] W. Lambrecht, A. Rodina, S. Limpijumnong, B. Segall, B. Meyer, Valence-band ordering and magneto-optic exciton fine structure in ZnO, Phys. Rev. B. 65 (2002) 075207. doi:10.1103/PhysRevB.65.075207.

[29] D.G. Thomas, The exciton spectrum of zinc oxide, J. Phys. Chem. Solids. 15 (1960) 86–96. doi:10.1016/0022-3697(60)90104-9.

[30] Y. Park, C. Litton, T. Collins, D. Reynolds, Exciton Spectrum of ZnO, Phys. Rev. 143 (1966) 512–519. doi:10.1103/PhysRev.143.512.

[31] S.L. Chen, W.M. Chen, I.A. Buyanova, Donor bound excitons involving a hole from the B valence band in ZnO: Time resolved and magneto-photoluminescence studies, Appl. Phys. Lett. 99 (2011) 091909. doi:https://doi.org/10.1063/1.3628332.

[32] C. Boemare, T. Monteiro, M.J. Soares, J.G. Guilherme, E. Alves, Photoluminescence studies in ZnO samples, Phys. B Condens. Matter. 308–310 (2001) 985–988. doi:10.1016/S0921-4526(01)00854-7.

[33] R. Pässler, E. Griebl, H. Riepl, G. Lautner, S. Bauer, H. Preis, W. Gebhardt, B. Buda, D.J. As, D. Schikora, K. Lischka, K. Papagelis, S. Ves, Temperature dependence of exciton peak energies in ZnS, ZnSe, and ZnTe epitaxial films, J. Appl. Phys. 86 (1999) 4403. doi:10.1063/1.371378.

[34] Y.P. Varshni, Temperature dependence of the energy gap in semiconductors, Physica. 34 (1967) 149–154. doi:10.1016/0031-8914(67)90062-6.
[35] M.O. Manasreh, Optical absorption near the band edge in GaN grown by metalorganic chemical-vapor deposition, Phys. Rev. B. 53 (1996) 16425. doi:https://doi.org/10.1103/PhysRevB.53.16425.
[36] A. Manoogian, J.C. Woolley, Temperature dependence of the energy gap in semiconductors, Can. J. Phys. 62 (1984) 285–287.
[37] L. Wang, N.C. Giles, Temperature dependence of the free-exciton transition energy in zinc oxide by photoluminescence excitation spectroscopy, J. Appl. Phys. 94 (2003) 973. doi:10.1063/1.1586977.
[38] J. Serrano, F.J. Manjón, A.H. Romero, A. Ivanov, R. Lauck, M. Cardona, M. Krisch, The phonon dispersion of wurtzite-ZnO revisited, Phys. Status Solidi. 244 (2007) 1478–1482. doi:10.1002/pssb.200675145.
[39] R. Cuscó, E. Alarcón-Lladó, J. Ibáñez, L. Artús, J. Jiménez, B. Wang, M. Callahan, Temperature dependence of Raman scattering in ZnO, Phys. Rev. B. 75 (2007) 165202. doi:10.1103/PhysRevB.75.165202.
[40] H. Harima, Properties of GaN and related compounds studied by means of Raman scattering, J. Phys. Condens. Matter. 14 (2002) R967–R993. doi:10.1088/0953-8984/14/38/201.
[41] Y. Gu, I.L. Kuskovsky, M. Yin, S. O'Brien, G.F. Neumark, Quantum confinement in ZnO nanorods, Appl. Phys. Lett. 85 (2004) 3833–3835. doi:10.1063/1.1811797.
[42] M. Yin, Y. Gu, I. Kuskovsky, Zinc oxide quantum rods, J. Am. Chem. Soc. 126 (2004) 6206–6207. doi:https://doi.org/10.1021/ja031696+.
[43] J. Rodrigues, T. Holz, R. Fath Allah, D. Gonzalez, T. Ben, M.R. Correira, T. Monteiro, F.M. Costa, Effect of the N2 and H2 plasma treatments on band edge emission of ZnO microrods, Sci. Rep. 5 (2015) 10783. doi:10.1038/srep10783.
[44] R. Calarco, T. Stoica, O. Brandt, L. Geelhaar, Surface-induced effects in GaN nanowires, J. Mater. Res. 26 (2011) 2157–2168. http://journals.cambridge.org/abstract_S0884291411002111 (accessed September 8, 2012).
[45] Z.N. Urgessa, J.R. Botha, M.O. Eriksson, C.M. Mbulanga, S.R. Dobson, S.R. Tankio Djiokap, K.F. Karlsson, V. Khranovskyy, R. Yakimova, P.-O. Holtz, Low temperature near band edge recombination dynamics in ZnO nanorods, J. Appl. Phys. 116 (2014) 123506. doi:10.1063/1.4896488.
[46] X. Fang, Y. Bando, U.K. Gautam, C. Ye, D. Golberg, Inorganic semiconductor nanostructures and their field-emission applications, J. Mater. Chem. 18 (2007) 509–522. doi:10.1039/B712874F.
[47] J.G. Lu, P. Chang, Z. Fan, Quasi-one-dimensional metal oxide materials—Synthesis, properties and applications, Mater. Sci. Eng. R Reports. 52 (2006) 49–91. doi:10.1016/j.mser.2006.04.002.
[48] R.R. Bacsa, J. Dexpert-Ghys, M. Verelst, A. Falqui, B. Machado, W.S. Bacsa, P. Chen, S.M. Zakeeruddin, M. Graetzel, P. Serp, Synthesis and Structure-Property Correlation in Shape-Controlled ZnO Nanoparticles Prepared by Chemical Vapor Synthesis and their Application in Dye-Sensitized Solar Cells, Adv. Funct. Mater. 19 (2009) 875–886. doi:10.1002/adfm.200801049.
[49] C.-H. Lee, W.-H. Chiu, K.-M. Lee, W.-H. Yen, H.-F. Lin, W.-F. Hsieh, J.-M. Wu, The influence of tetrapod-like ZnO morphology and electrolytes on energy conversion efficiency of dye-sensitized solar cells, Electrochim. Acta. 55 (2010) 8422–8429. doi:10.1016/j.electacta.2010.07.061.

[50] J. Rodrigues, A.F.R. Cerqueira, M.G. Sousa, N.F. Santos, A. Pimentel, E. Fortunato, A.F. da Cunha, T. Monteiro, F.M. Costa, Exploring the potential of laser assisted flow deposition grown ZnO for photovoltaic applications, Mater. Chem. Phys. 177 (2016) 322–329. doi:10.1016/j.matchemphys.2016.04.033.
[51] Y.K. Mishra, R. Adelung, ZnO tetrapod materials for functional applications, Mater. Today. 21 (2017) 631–651. doi:10.1016/J.MATTOD.2017.11.003.
[52] Y.F. Hsu, Y.Y. Xi, C.T. Yip, A.B. Djurišić, W.K. Chan, Dye-sensitized solar cells using ZnO tetrapods, J. Appl. Phys. 103 (2008) 083114. doi:10.1063/1.2909907.
[53] Q. Zhang, G. Cao, Nanostructured photoelectrodes for dye-sensitized solar cells, Nano Today. 6 (2011) 91–109. doi:10.1016/j.nantod.2010.12.007.
[54] A.B. Djurišić, Y.H. Leung, K.H. Tam, Y.F. Hsu, L. Ding, W.K. Ge, Y.C. Zhong, K.S. Wong, W.K. Chan, H.L. Tam, K.W. Cheah, W.M. Kwok, D.L. Phillips, Defect emissions in ZnO nanostructures, Nanotechnology. 18 (2007) 095702. doi:10.1088/0957-4484/18/9/095702.
[55] A. Janotti, C.G. Van De Walle, Native point defects in ZnO, Phys. Rev. B - Condens. Matter Mater. Phys. 76 (2007) 165202. doi:10.1103/PhysRevB.76.165202.
[56] A. Janotti, C.G. Van De Walle, New insights into the role of native point defects in ZnO, J. Cryst. Growth. 287 (2006) 58–65. doi:10.1016/j.jcrysgro.2005.10.043.
[57] L.M. Kukreja, P. Misra, J. Fallert, D.M. Phase, H. Kalt, Correlation of spectral features of photoluminescence with residual native defects of ZnO thin films annealed at different temperatures, J. Appl. Phys. 112 (2012) 013525. doi:10.1063/1.4730774.
[58] D.P. Norton, Y.W. Heo, M.P. Ivill, K. Ip, S.J. Pearton, M.F. Chisholm, T. Steiner, ZnO: growth, doping & processing, Mater. Today. 7 (2004) 34–40.
[59] R. Vidya, P. Ravindran, H. Fjellvåg, B.G. Svensson, E. Monakhov, M. Ganchenkova, N.R. M., Energetics of intrinsic defects and their complexes in ZnO investigated by density functional calculations, Phys. Rev. B. 83 (2011) 045206.
[60] X.J. Wang, L.S. Vlasenko, S.J. Pearton, W.M. Chen, I.A. Buyanova, Oxygen and zinc vacancies in as-grown ZnO single crystals, J. Phys. D. Appl. Phys. 42 (2009) 175411. doi:10.1088/0022-3727/42/17/175411.
[61] M.D. McCluskey, S.J. Jokela, Defects in ZnO, J. Appl. Phys. 106 (2009) 071101. doi:https://doi.org/10.1063/1.3216464.
[62] F. Oba, M. Choi, A. Togo, I. Tanaka, Point defects in ZnO: an approach from first principles, Sci Technol Adv Mater. 12 (2011) 034302. doi:10.1088/1468-6996/12/3/034302.
[63] D.K. Schroder, Semiconductor Material and Device Characterization, John Wiley & Sons, 2006.
[64] C.F. Klingshirn, Semiconductor Optics, Springer, 2007.
[65] P.Y. Yu, M. Cardona, Fundamentals of Semiconductors, Springer Berlin Heidelberg, Berlin, Heidelberg, 2005. doi:10.1007/b137661.
[66] C.R. Ronda, Luminescence: from theory to applications, Wiley-VCH, 2008. http://books.google.pt/books?id=o9CDdfrV8eoC.
[67] B. Henderson, G.F. Imbusch, Optical Spectroscopy of Inorganic Solids, Oxford University Press, 2006. https://books.google.com/books?id=_EypTNBm2aQC&pgis=1 (accessed April 6, 2015).
[68] S. Tsoi, X. Lu, A.K. Ramdas, H. Alawadhi, M. Grimsditch, M. Cardona, R.

Lauck, Isotopic-mass dependence of the A, B, and C excitonic band gaps in ZnO at low temperatures, Phys. Rev. B. 74 (2006) 165203. doi:https://doi.org/10.1103/PhysRevB.74.165203.

[69] K. Lischka, A. Waag, H. Mariette, J. Neugebauer, M.R. Wagner, H.W. Kunert, A.G.J. Machatine, A. Hoffmann, P. Niyongabo, J. Malherbe, J. Barnas, Bound and free excitons in ZnO. Optical selection rules in the absence and presence of time reversal symmetry, Microelectronics J. 40 (2009) 289–292.

[70] J.F. Muth, R.M. Kolbas, A.K. Sharma, S. Oktyabrsky, J. Narayan, Excitonic structure and absorption coefficient measurements of ZnO single crystal epitaxial films deposited by pulsed laser deposition, J. Appl. Phys. 85 (1999) 7884. doi:10.1063/1.370601.

[71] B.K. Meyer, H. Alves, D.M. Hofmann, W. Kriegseis, D. Forster, F. Bertram, J. Christen, A. Hoffmann, M. Straßburg, M. Dworzak, U. Haboeck, A. V. Rodina, Bound exciton and donor–acceptor pair recombinations in ZnO, Phys. Status Solidi. 241 (2004) 231–260. doi:10.1002/pssb.200301962.

[72] T. Monteiro, A.J. Neves, M.C. Carmo, M.J. Soares, M. Peres, J. Wang, E. Alves, E. Rita, U. Wahl, Near-band-edge slow luminescence in nominally undoped bulk ZnO, J. Appl. Phys. 98 (2005) 013502. doi:10.1063/1.1946200.

[73] M.A. Reshchikov, H. Morkoç, Luminescence properties of defects in GaN, J. Appl. Phys. 97 (2005) 061301-061301–95. doi:doi:10.1063/1.1868059.

[74] B. Monemar, P.P. Paskov, J.P. Bergman, A.A. Toropov, T. V. Shubina, T. Malinauskas, A. Usui, Recombination of free and bound excitons in GaN, Phys. Status Solidi. 245 (2008) 1723–1740. doi:10.1002/pssb.200844059.

[75] K. Thonke, T. Gruber, N. Teofilov, R. Schönfelder, A. Waag, R. Sauer, Donor–acceptor pair transitions in ZnO substrate material, Phys. B Condens. Matter. 308 (2001) 945–948. http://www.sciencedirect.com/science/article/pii/S0921452601008778 (accessed November 27, 2013).

[76] V.S. Yalishev, Y.S. Kim, X.L. Deng, B.H. Park, S.U. Yuldashev, Study of the photoluminescence emission line at 3.33 eV in ZnO films, J. Appl. Phys. 112 (2012) 013528. doi:10.1063/1.4733952.

[77] A. Walsh, J.L.F. Da Silva, S.-H. Wei, Origins of band-gap renormalization in degenerately doped semiconductors, Phys. Rev. B. 78 (2008) 075211. doi:10.1103/PhysRevB.78.075211.

[78] Q. Yan, P. Rinke, M. Winkelnkemper, A. Qteish, D. Bimberg, M. Scheffler, C.G. Van de Walle, Band parameters and strain effects in ZnO and group-III nitrides, Semicond. Sci. Technol. 26 (2011) 014037. doi:10.1088/0268-1242/26/1/014037.

[79] A. Janotti, C.G. Van De Walle, Fundamentals of zinc oxide as a semiconductor, Reports Prog. Phys. 72 (2009) 126501. doi:10.1088/0034-4885/72/12/126501.

[80] P.J. Dean, Bound excitons and donor-acceptor pairs in natural and synthetic diamond, Phys. Rev. 139 (1965) A588. doi:https://doi.org/10.1103/PhysRev.139.A588.

[81] A. Zeuner, H. Alves, J. Sann, W. Kriegseis, C. Neumann, D.M. Hofmann, B.K. Meyer, A. Hoffmann, U. Haboeck, M. Straßburg, A. Kaschner, Nitrogen doping in bulk and epitaxial ZnO, Phys. Status Solidi. 1 (2004) 731–734. doi:10.1002/pssc.200304255.

[82] A. Zeuner, H. Alves, D.M. Hofmann, B.K. Meyer, A. Hoffmann, U. Haboeck, M. Strassburg, M. Dworzak, Optical Properties of the Nitrogen Acceptor in Epitaxial ZnO, Phys. Status Solidi. 234 (2002) R7–R9. doi:https://doi.org/10.1002/1521-3951(200212)234:3<R7::AID-PSSB99997>3.0.CO;2-D.

[83] B.K. Meyer, ZnO: acceptor binding energies, in: Semicond. Landolt-Börnstein - Gr. III 'Condensed Matter, 2011: pp. 597–600. doi:10.1007/978-3-642-14148-5_334.
[84] I. Pelant, J. Valenta, Luminescence Spectroscopy of Semiconductors, OUP Oxford, 2012.
[85] Y.W. Heo, D.P. Norton, S.J. Pearton, Origin of green luminescence in ZnO thin film grown by molecular-beam epitaxy, J. Appl. Phys. 98 (2005) 073502. doi:10.1063/1.2064308.
[86] T. Monteiro, M.J. Soares, A. Neves, S. Pereira, M.R. Correia, M. Peres, E. Alves, D. Rogers, F. Teherani, V. Munoz-SanJose, T. Trindade, A. Pereira, Optical active centres in ZnO samples, J. Non. Cryst. Solids. 352 (2006) 1453–1456. doi:10.1016/j.jnoncrysol.2005.10.034.
[87] M.A. Reshchikov, H. Morkoç, B. Nemeth, J. Nause, J. Xie, B. Hertog, A. Osinsky, Luminescence properties of defects in ZnO, Phys. B Condens. Matter. 401–402 (2007) 358–361. doi:10.1016/j.physb.2007.08.187.
[88] B. Lin, Z. Fu, Y. Jia, Green luminescent center in undoped zinc oxide films deposited on silicon substrates, Appl. Phys. Lett. 79 (2001) 943. doi:10.1063/1.1394173.
[89] F.H. Leiter, H.R. Alves, A. Hofstaetter, D.M. Hofmann, B.K. Meyer, The Oxygen Vacancy as the Origin of a Green Emission in Undoped ZnO, Phys. Status Solidi. 226 (2001) R4–R5. doi:10.1002/1521-3951(200107)226:1<R4::AID-PSSB99994>3.0.CO;2-F.
[90] T. Sekiguchi, S. Miyashita, K. Obar, T. Shishido, N. Sakagami, Hydrothermal growth of ZnO single crystals and their optical characterization, J. Cryst. Growth. 214–215 (2000) 72–76. doi:https://doi.org/10.1016/S0022-0248(00)00065-8.
[91] C.H. Ahn, Y.Y. Kim, D.C. Kim, S.K. Mohanta, H.K. Cho, A comparative analysis of deep level emission in ZnO layers deposited by various methods, J. Appl. Phys. 105 (2009) 013502. doi:10.1063/1.3054175.
[92] R. Dingle, Luminescent Transitions Associated With Divalent Copper Impurities and the Green Emission from Semiconducting Zinc Oxide, Phys. Rev. Lett. 23 (1969) 579–581. doi:10.1103/PhysRevLett.23.579.
[93] D. Byrne, F. Herklotz, M.O. Henry, E. McGlynn, Unambiguous identification of the role of a single Cu atom in the ZnO structured green band., J. Phys. Condens. Matter. 24 (2012) 215802. doi:10.1088/0953-8984/24/21/215802.
[94] A.F. Kohan, G. Ceder, D. Morgan, C.G. Van De Walle, First-principles study of native point defects in ZnO, Phys. Rev. B. 61 (2000) 19–27. doi:10.1103/PhysRevB.61.15019.
[95] R. Kuhnert, R. Helbig, Vibronic structure of the green photoluminescence due to copper impurities in ZnO, J. Lumin. 26 (1981) 203–206. doi:10.1016/0022-2313(81)90182-4.
[96] J. Solé, L. Bausa, D. Jaque, An Introduction to the Optical Spectroscopy of Inorganic Solids, John Wiley & Sons, 2005.
[97] M.A. Reshchikov, J.Q. Xie, B. Hertog, A. Osinsky, Yellow luminescence in ZnO layers grown on sapphire, J. Appl. Phys. 103 (2008) 103514. doi:10.1063/1.2924437.
[98] F.H. Leiter, H.R. Alves, A. Hofstaetter, D.M. Hofmann, B.K. Meyer, The Oxygen Vacancy as the Origin of a Green Emissionin Undoped ZnO, Phys. Status Solidi - Rapid Res. Note. 226 (2001) R4– R5.
[99] F. Leiter, Magnetic resonance experiments on the green emission in undoped ZnO crystals, Phys. B Condens. Matter. 308–310 (2001) 908–911.

doi:10.1016/S0921-4526(01)00837-7.
[100] C. Gaspar, F. Costa, T. Monteiro, Optical characterization of ZnO, J. Mater. Sci. Mater. Electron. 12 (2001) 269–271.
[101] H. Priller, M. Decker, R. Hauschild, H. Kalt, C. Klingshirn, Macroscopic energy transport in ZnO monitored by spatiotemporally resolved luminescence, Appl. Phys. Lett. 86 (2005) 111909. doi:10.1063/1.1882746.
[102] N. Zhou, B.C. Hu, Q.Y. Zhang, C.Y. Ma, S.Z. Hao, New fine structure of red luminescence in ZnO observed under exciton resonance excitation, AIP Adv. 9 (2019) 045004. doi:10.1063/1.5091068.
[103] L.J. Brillson, Y. Dong, F. Tuomisto, B.G. Svensson, A.Y. Kuznetsov, D. Doutt, H.L. Mosbacker, G. Cantwell, J. Zhang, J.J. Song, Z.-Q. Fang, D.C. Look, Native point defects at ZnO surfaces, interfaces and bulk films, Phys. Status Solidi. 9 (2012) 1566–1569. doi:10.1002/pssc.201100538.
[104] J. Lv, C. Li, Z. Chai, Defect luminescence and its mediated physical properties in ZnO, J. Lumin. 208 (2019) 225–237. doi:10.1016/j.jlumin.2018.12.050.
[105] A.A. Sokol, S.A. French, S.T. Bromley, C.C.A. Richard, H.J.J. van Dam, P. Sherwood, Point defects in ZnO, Faraday Discuss. 134 (2007) 267–282. doi:https://doi.org/10.1039/B607406E.
[106] X. Zhou, Q. Kuang, Z.-Y. Jiang, Z.-X. Xie, T. Xu, R.-B. Huang, L.-S. Zheng, The Origin of Green Emission of ZnO Microcrystallites: Surface-Dependent Light Emission Studied by Cathodoluminescence, J. Phys. Chem. C. 111 (2007) 12091–12093. doi:10.1021/jp071928h.
[107] Z.-M. Liao, H.-Z. Zhang, Y.-B. Zhou, J. Xu, J.-M. Zhang, D.-P. Yu, Surface effects on photoluminescence of single ZnO nanowires, Phys. Lett. A. 372 (2008) 4505–4509. doi:10.1016/j.physleta.2008.04.013.
[108] Z. Fan, D. Wang, P.-C. Chang, W.-Y. Tseng, J.G. Lu, ZnO nanowire field-effect transistor and oxygen sensing property, Appl. Phys. Lett. 85 (2004) 5923. doi:https://doi.org/10.1063/1.1836870.
[109] V. Chakrapani, C. Pendyala, K. Kash, A.B. Anderson, M.K. Sunkara, J.C. Angus, Electrochemical Pinning of the Fermi Level: Mediation of Photoluminescence from Gallium Nitride and Zinc Oxide, J. Am. Chem. Soc. 130 (2008) 12944–12952. doi:10.1021/ja710999r.
[110] C.-Y. Chen, J.R.D. Retamal, I.-W. Wu, D.-H. Lien, M.-W. Chen, Y. Ding, Y.-L. Chueh, C.-I. Wu, J.-H. He, Probing Surface Band Bending of Surface-Engineered Metal Oxide Nanowires, ACS Nano. 6 (2012) 9366–9372. doi:10.1021/nn205097e.
[111] L. Brillson, J. Cox, H. Gao, G. Foster, W. Ruane, A. Jarjour, M. Allen, D. Look, H. von Wenckstern, M. Grundmann, Native Point Defect Measurement and Manipulation in ZnO Nanostructures, Materials (Basel). 12 (2019) 2242. doi:https://doi.org/10.3390/ma12142242.
[112] R. Calarco, M. Marso, T. Richter, A.I. Aykanat, R. Meijers, A. V D Hart, T. Stoica, H. Lüth, Size-dependent photoconductivity in MBE-grown GaN-nanowires., Nano Lett. 5 (2005) 981–4. doi:10.1021/nl0500306.
[113] Z. Zhang, J.T. Yates, Band Bending in Semiconductors: Chemical and Physical Consequences at Surfaces and Interfaces, Chem. Rev. 112 (2012) 5520–5551. doi:10.1021/cr3000626.
[114] K.M. Wong, S.M. Alay-e-Abbas, Y. Fang, A. Shaukat, Y. Lei, Spatial distribution of neutral oxygen vacancies on ZnO nanowire surfaces: An investigation combining confocal microscopy and first principles calculations, J. Appl. Phys. 114 (2013) 034901. doi:https://doi.org/10.1063/1.4813517.

[115] D. Li, Y.H. Leung, A.B. Djurišić, Z.T. Liu, M.H. Xie, S.L. Shi, S.J. Xu, W.K. Chan, Different origins of visible luminescence in ZnO nanostructures fabricated by the chemical and evaporation methods, Appl. Phys. Lett. 85 (2004) 1601–1603. doi:10.1063/1.1786375.
[116] K.H. Tam, C.K. Cheung, Y.H. Leung, A.B. Djurišić, C.C. Ling, C.D. Beling, S. Fung, W.M. Kwok, W.K. Chan, D.L. Phillips, L. Ding, W.K. Ge, Defects in ZnO nanorods prepared by a hydrothermal method, J. Phys. Chem. B. 110 (2006) 20865–20871. doi:10.1021/jp063239w.
[117] A.B. Djurišić, Y.H. Leung, K.H. Tam, L. Ding, W.K. Ge, H.Y. Chen, S. Gwo, Green, yellow, and orange defect emission from ZnO nanostructures: Influence of excitation wavelength, Appl. Phys. Lett. 88 (2006) 103107. doi:10.1063/1.2182096.
[118] V.A.L. Roy, A.B. Djurišić, W.K. Chan, J. Gao, H.F. Lui, C. Surya, Luminescent and structural properties of ZnO nanorods prepared under different conditions, Appl. Phys. Lett. 83 (2003) 141–143. doi:10.1063/1.1589184.
[119] A.B. Djurisić, Y.H. Leung, Optical properties of ZnO nanostructures., Small. 2 (2006) 944–61. doi:10.1002/smll.200600134.
[120] Y.H. Leung, A.B. Djurišić, Z.T. Liu, D. Li, M.H. Xie, W.K. Chan, Defect photoluminescence of ZnO nanorods synthesized by chemical methods, J. Phys. Chem. Solids. 69 (2008) 353–357. doi:10.1016/j.jpcs.2007.07.029.
[121] L.E. Greene, M. Law, J. Goldberger, F. Kim, J.C. Johnson, Y. Zhang, R.J. Saykally, P. Yang, Low-temperature wafer-scale production of ZnO nanowire arrays., Angew. Chem. Int. Ed. Engl. 42 (2003) 3031–4. doi:10.1002/anie.200351461.
[122] X.L. Wu, G.G. Siu, C.L. Fu, H.C. Ong, Photoluminescence and cathodoluminescence studies of stoichiometric and oxygen-deficient ZnO films, Appl. Phys. Lett. 78 (2001) 2285. doi:10.1063/1.1361288.
[123] J.W.P. Hsu, D.R. Tallant, R.L. Simpson, N.A. Missert, R.G. Copeland, Luminescent properties of solution-grown ZnO nanorods, Appl. Phys. Lett. 88 (2006) 252103. doi:10.1063/1.2214137.
[124] H. Zhou, H. Alves, D.M. Hofmann, W. Kriegseis, B.K. Meyer, G. Kaczmarczyk, A. Hoffmann, Behind the weak excitonic emission of ZnO quantum dots: ZnO/Zn(OH)[sub 2] core-shell structure., Appl. Phys. Lett. 80 (2002) 210.
[125] N.E. Hsu, W.K. Hung, Y.F. Chen, Origin of defect emission identified by polarized luminescence from aligned ZnO nanorods, J. Appl. Phys. 96 (2004) 4671–4673. doi:10.1063/1.1787905.
[126] F. Fabbri, M. Villani, A. Catellani, A. Calzolari, G. Cicero, D. Calestani, G. Calestani, A. Zappettini, B. Dierre, T. Sekiguchi, G. Salviati, Zn vacancy induced green luminescence on non-polar surfaces in ZnO nanostructures, Sci. Rep. 4 (2015) 5158. doi:10.1038/srep05158.
[127] I. Shalish, H. Temkin, V. Narayanamurti, Size-dependent surface luminescence in ZnO nanowires, Phys. Rev. B. 69 (2004) 245401. doi:10.1103/PhysRevB.69.245401.
[128] J. Grabowska, A. Meaney, K.K. Nanda, J.-P. Mosnier, M.O. Henry, J.-R. Duclère, E. McGlynn, Surface excitonic emission and quenching effects in ZnO nanowire/nanowall systems: Limiting effects on device potential, Phys. Rev. B. 71 (2005) 115439. doi:10.1103/PhysRevB.71.115439.
[129] M. Biswas, Y.S. Jung, H.K. Kim, K. Kumar, G.J. Hughes, S. Newcomb, M.O. Henry, E. McGlynn, Microscopic origins of the surface exciton photoluminescence peak in ZnO nanostructures, Phys. Rev. B. 83 (2011) 235320.

doi:10.1103/PhysRevB.83.235320.
[130] M. Norek, Approaches to enhance UV light emission in ZnO nanomaterials, Curr. Appl. Phys. 19 (2019) 867–883. doi:10.1016/j.cap.2019.05.006.
[131] C. Chen, H. He, Y. Lu, K. Wu, Z. Ye, Surface passivation effect on the Photoluminescence of ZnO nanorods, ACS Appl. Mater. Interfaces. 5 (2013) 6354–6359. http://pubs.acs.org/doi/abs/10.1021/am401418b (accessed July 26, 2013).
[132] S. Anantachaisilp, S.M. Smith, C. Ton-That, T. Osotchan, A.R. Moon, M.R. Phillips, Tailoring Deep Level Surface Defects in ZnO Nanorods for High Sensitivity Ammonia Gas Sensing, J. Phys. Chem. C. 118 (2014) 27150–27156. doi:10.1021/jp5085857.
[133] X. Zhang, Y. Xia, T. He, Tuning photoluminescence properties of ZnO nanorods via surface modification, Mater. Chem. Phys. 137 (2012) 622–627. doi:10.1016/j.matchemphys.2012.09.065.
[134] S.C. Singh, R. Gopal, Drop shaped zinc oxide quantum dots and their self-assembly into dendritic nanostructures: Liquid assisted pulsed laser ablation and characterizations, Appl. Surf. Sci. 258 (2012) 2211–2218. doi:10.1016/j.apsusc.2011.05.018.
[135] M. Schirra, R. Schneider, A. Reiser, G.M. Prinz, M. Feneberg, J. Biskupek, U. Kaiser, C.E. Krill, K. Thonke, R. Sauer, Stacking fault related 3.31-eV luminescence at 130-meV acceptors in zinc oxide, Phys. Rev. B. 77 (2008) 125215. doi:10.1103/PhysRevB.77.125215.
[136] M. Schirra, A. Reiser, G.M. Prinz, A. Ladenburger, K. Thonke, R. Sauer, Cathodoluminescence study of single zinc oxide nanopillars with high spatial and spectral resolution, J. Appl. Phys. 101 (2007) 113509. doi:10.1063/1.2735411.
[137] K. Thonke, M. Schirra, R. Schneider, A. Reiser, G.M. Prinz, M. Feneberg, J. Biskupek, U. Kaiser, R. Sauer, The role of stacking faults and their associated 0.13ev acceptor state in doped and undoped ZnO layers and nanostructures, Microelectronics J. 40 (2009) 210–214. doi:10.1016/j.mejo.2008.07.031.
[138] J. Fallert, R. Hauschild, F. Stelzl, A. Urban, M. Wissinger, H. Zhou, C. Klingshirn, H. Kalt, Surface-state related luminescence in ZnO nanocrystals, J. Appl. Phys. 101 (2007) 073506. doi:10.1063/1.2718290.
[139] D. Tainoff, B. Masenelli, P. Melinon, A. Belsky, G. Ledoux, D. Amans, C. Dujardin, N. Fedorov, P. Martin, Probing the excitonic emission of ZnO nanoparticles using UV–VUV excitations, J. Lumin. 129 (2009) 1798–1801. doi:10.1016/j.jlumin.2009.04.099.
[140] D. Tainoff, B. Masenelli, P. Mélinon, A. Belsky, G. Ledoux, D. Amans, C. Dujardin, N. Fedorov, P. Martin, Competition between exciton-phonon interaction and defects states in the 3.31 eV band in ZnO, Phys. Rev. B. 81 (2010) 115304. doi:10.1103/PhysRevB.81.115304.
[141] T. Børseth, F. Tuomisto, J. Christensen, E. Monakhov, B. Svensson, A. Kuznetsov, Vacancy clustering and acceptor activation in nitrogen-implanted ZnO, Phys. Rev. B. 77 (2008) 045204. doi:10.1103/PhysRevB.77.045204.
[142] J. Rodrigues, A. Pimentel, E. Fortunato, T. Monteiro, F.M. Costa, Photocatalytic Activity of Laser-Processed ZnO Micro/Nanocrystals, Phys. Status Solidi. 215 (2018) 1800155. doi:10.1002/pssa.201800155.
[143] J. Rodrigues, D. Smazna, N. Ben Sedrine, E. Nogales, R. Adelung, Y.K. Mishra, B. Mendez, M.R. Correia, T. Monteiro, Probing surface states in C60 decorated ZnO microwires: detailed photoluminescence and cathodoluminescence investigations, Nanoscale Adv. 1 (2019) 1516–1526. doi:10.1039/c8na00296g.

[144] J. Rodrigues, D. Mata, A. Pimentel, D. Nunes, R. Martins, E. Fortunato, A.J. Neves, T. Monteiro, F.M. Costa, One-step synthesis of ZnO decorated CNT buckypaper composites and their optical and electrical properties, Mater. Sci. Eng. B. 195 (2015) 38–44. doi:10.1016/j.mseb.2015.01.009.

[145] J. Rodrigues, D. Mata, A.J.S. Fernandes, M.A. Neto, R.F. Silva, T. Monteiro, F.M. Costa, ZnO nanostructures grown on vertically aligned carbon nanotubes by laser-assisted flow deposition, Acta Mater. 60 (2012) 5143–5150. doi:10.1016/j.actamat.2012.06.005.

[146] L. El Mir, A. Amlouk, C. Barthou, S. Alaya, Synthesis and luminescence properties of ZnO/Zn2SiO4/SiO2 composite based on nanosized zinc oxide-confined silica aerogels, Phys. B Condens. Matter. 388 (2007) 412–417. doi:10.1016/j.physb.2006.06.151.

[147] M. Achermann, Exciton−Plasmon Interactions in Metal−Semiconductor Nanostructures, J. Phys. Chem. Lett. 1 (2010) 2837–2843. doi:10.1021/jz101102e.

[148] T. Chen, G.Z. Xing, Z. Zhang, H.Y. Chen, T. Wu, Tailoring the photoluminescence of ZnO nanowires using Au nanoparticles, Nanotechnology. 19 (2008) 435711. doi:10.1088/0957-4484/19/43/435711.

[149] D. Smazna, J. Rodrigues, S. Shree, V. Postica, G. Neubüser, A.F. Martins, N. Ben Sedrine, N.K. Jena, L. Siebert, F. Schütt, O. Lupan, R. Ahuja, M.R. Correia, T. Monteiro, L. Kienle, Y. Yang, R. Adelung, Y.K. Mishra, Buckminsterfullerene hybridized zinc oxide tetrapods: Defects and charge transfer induced optical and electrical response, Nanoscale. 10 (2018) 10050–10062. doi:10.1039/c8nr01504j.

[150] S. Guha, J. Menéndez, J.B. Page, G.B. Adams, G.S. Spencer, J.P. Lehman, P. Giannozzi, S. Baroni, Isotopically resolved Raman spectra of C 60, Phys. Rev. Lett. 72 (1994) 3359–3362. doi:10.1103/PhysRevLett.72.3359.

[151] O. Lupan, F. Schütt, V. Postica, D. Smazna, Y.K. Mishra, R. Adelung, Sensing performances of pure and hybridized carbon nanotubes-ZnO nanowire networks: A detailed study, Sci. Rep. 7 (2017) 14715. doi:10.1038/s41598-017-14544-0.

[152] M. Sharma, M. Joshi, S. Nigam, S. Shree, D.K. Avasthi, R. Adelung, S.K. Srivastava, Y. Kumar Mishra, ZnO tetrapods and activated carbon based hybrid composite: Adsorbents for enhanced decontamination of hexavalent chromium from aqueous solution, Chem. Eng. J. 358 (2019) 540–551. doi:10.1016/j.cej.2018.10.031.

[153] J. Rodrigues, J. Zanoni, G. Gaspar, A.J.S. Fernandes, A.F. Carvalho, N.F. Santos, T. Monteiro, F.M. Costa, ZnO decorated laser-induced graphene produced by direct laser scribing, Nanoscale Adv. 1 (2019) 3252–3268. doi:10.1039/C8NA00391B.

[154] C. Jin, H. Kim, H.-Y. Ryu, H.W. Kim, C. Lee, Subwavelength Optical Resonant Cavity-Induced Enhancement of the Near-Band-Edge Emission from ZnO-Core/SnO 2 -Shell Nanorods, J. Phys. Chem. C. 115 (2011) 8513–8518. doi:10.1021/jp2000514.

[155] J.M. Lin, C.L. Cheng, H.Y. Lin, Y.F. Chen, Giant enhancement of band edge emission in ZnO and SnO nanocomposites, Opt. Lett. 31 (2006) 3173. doi:10.1364/OL.31.003173.

[156] A. Pimentel, J. Rodrigues, P. Duarte, D. Nunes, F.M. Costa, T. Monteiro, R. Martins, E. Fortunato, Effect of solvents on ZnO nanostructures synthesized by solvothermal method assisted by microwave radiation: a photocatalytic study, J. Mater. Sci. 50 (2015) 5777–5787. doi:10.1007/s10853-015-9125-7.

[157] A.B. Djurišić, X. Liu, Y.H. Leung, Zinc oxide films and nanomaterials for photovoltaic applications, Phys. Status Solidi - Rapid Res. Lett. 8 (2014) 123–132. doi:10.1002/pssr.201300103.
[158] F. Liu, Y.H. Leung, A.B. Djurišić, A.M.C. Ng, W.K. Chan, Native Defects in ZnO: Effect on Dye Adsorption and Photocatalytic Degradation, J. Phys. Chem. C. 117 (2013) 12218–12228. doi:10.1021/jp403478q.
[159] A. Tereshchenko, M. Bechelany, R. Viter, V. Khranovskyy, V. Smyntyna, N. Starodub, R. Yakimova, Optical biosensors based on ZnO nanostructures: Advantages and perspectives. A review, Sensors Actuators, B Chem. 229 (2016) 664–677. doi:10.1016/j.snb.2016.01.099.
[160] X. Liu, Y. Sun, M. Yu, Y. Yin, B. Du, W. Tang, T. Jiang, B. Yang, W. Cao, M.N.R. Ashfold, Enhanced ethanol sensing properties of ultrathin ZnO nanosheets decorated with CuO nanoparticles, Sensors Actuators, B Chem. 255 (2018) 3384–3390. doi:10.1016/j.snb.2017.09.165.
[161] G. Lu, J. Xu, J. Sun, Y. Yu, Y. Zhang, F. Liu, UV-enhanced room temperature NO2 sensor using ZnO nanorods modified with SnO2 nanoparticles, Sensors Actuators, B Chem. 162 (2012) 82–88. doi:10.1016/j.snb.2011.12.039.
[162] C.F. Klingshirn, B.K. Meyer, A. Waag, A. Hoffmann, J.M.M. Geurts, ZnO: From Fundamental Properties Towards Novel Applications, Springer, 2010. http://books.google.com/books?id=TYXinw6pKk4C.
[163] Yong-Seok Choi, Jang-Won Kang, Dae-Kue Hwang, Seong-Ju Park, Recent Advances in ZnO-Based Light-Emitting Diodes, Electron Devices, IEEE Trans. 57 (2010) 26–41. doi:10.1109/TED.2009.2033769.
[164] D. Nunes, A. Pimentel, A. Gonçalves, S. Pereira, R. Branquinho, P. Barquinha, E. Fortunato, R. Martins, Metal oxide nanostructures for sensor applications, Semicond. Sci. Technol. 34 (2019) 043001. doi:10.1088/1361-6641/ab011e.
[165] M. Hoppe, O. Lupan, V. Postica, N. Wolff, V. Duppel, L. Kienle, I. Tiginyanu, R. Adelung, ZnAl2O4-Functionalized Zinc Oxide Microstructures for Highly Selective Hydrogen Gas Sensing Applications, Phys. Status Solidi Appl. Mater. Sci. 215 (2018) 1700772. doi:10.1002/pssa.201700772.
[166] D. Gedamu, I. Paulowicz, S. Kaps, O. Lupan, S. Wille, G. Haidarschin, Y.K. Mishra, R. Adelung, Rapid Fabrication Technique for Interpenetrated ZnO Nanotetrapod Networks for Fast UV Sensors, Adv. Mater. 26 (2014) 1541–1550. doi:10.1002/adma.201304363.
[167] K.K. Wong, A. Ng, X.Y. Chen, Y.H. Ng, Y.H. Leung, K.H. Ho, A.B. Djurišić, A.M.C. Ng, W.K. Chan, L. Yu, D.L. Phillips, Effect of ZnO nanoparticle properties on dye-sensitized solar cell performance., ACS Appl. Mater. Interfaces. 4 (2012) 1254–61. doi:10.1021/am201424d.
[168] E.M.C. Fortunato, P.M.C. Barquinha, A.C.M.B.G. Pimentel, A.M.F. Gonçalves, A.J.S. Marques, L.M.N. Pereira, R.F.P. Martins, Fully Transparent ZnO Thin-Film Transistor Produced at Room Temperature, Adv. Mater. 17 (2005) 590–594. doi:10.1002/adma.200400368.
[169] A. Mallick, D. Basak, Revisiting the electrical and optical transmission properties of co-doped ZnO thin films as n-type TCOs, Prog. Mater. Sci. 96 (2018) 86–110. doi:10.1016/j.pmatsci.2018.03.004.
[170] J. Hu, R.G. Gordon, Textured aluminum-doped zinc oxide thin films from atmospheric pressure chemical-vapor deposition, J. Appl. Phys. 71 (1992) 880–890. doi:10.1063/1.351309.
[171] O. Nakagawara, Y. Kishimoto, H. Seto, Y. Koshido, Y. Yoshino, T. Makino, Moisture-resistant ZnO transparent conductive films with Ga heavy doping,

Appl. Phys. Lett. 89 (2006) 091904. doi:10.1063/1.2337542.
[172] M.-C. Jun, S.-U. Park, J.-H. Koh, Comparative studies of Al-doped ZnO and Ga-doped ZnO transparent conducting oxide thin films, Nanoscale Res. Lett. 7 (2012) 639. doi:10.1186/1556-276X-7-639.
[173] C.E. Benouis, M. Benhaliliba, A. Sanchez Juarez, M.S. Aida, F. Chami, F. Yakuphanoglu, The effect of indium doping on structural, electrical conductivity, photoconductivity and density of states properties of ZnO films, J. Alloys Compd. 490 (2010) 62–67. doi:10.1016/j.jallcom.2009.10.098.
[174] C.G. Van de Walle, Hydrogen as a Cause of Doping in Zinc Oxide, Phys. Rev. Lett. 85 (2000) 1012–1015. doi:10.1103/PhysRevLett.85.1012.
[175] B.E. Sernelius, K.-F. Berggren, Z.-C. Jin, I. Hamberg, C.G. Granqvist, Band-gap tailoring of ZnO by means of heavy Al doping, Phys. Rev. B. 37 (1988) 10244–10248. doi:10.1103/PhysRevB.37.10244.
[176] H.. Lee, S.. Lau, Y.. Wang, K.. Tse, H.. Hng, B.. Tay, Structural, electrical and optical properties of Al-doped ZnO thin films prepared by filtered cathodic vacuum arc technique, J. Cryst. Growth. 268 (2004) 596–601. doi:10.1016/j.jcrysgro.2004.04.098.
[177] J.G. Lu, S. Fujita, T. Kawaharamura, H. Nishinaka, Y. Kamada, T. Ohshima, Z.Z. Ye, Y.J. Zeng, Y.Z. Zhang, L.P. Zhu, H.P. He, B.H. Zhao, Carrier concentration dependence of band gap shift in n-type ZnO:Al films, J. Appl. Phys. 101 (2007) 083705. doi:10.1063/1.2721374.
[178] T. Frade, D. Siopa, A.F. Martins, J.F.C. Carreira, J. Rodrigues, N. Ben Sedrine, M.R. Correia, T. Monteiro, R. Tena-Zaera, A. Gomes, Optoelectronic Characterization of ZnO Nanorod Arrays Obtained by Pulse Electrodeposition, J. Electrochem. Soc. 165 (2018) D595–D603. doi:10.1149/2.0131813jes.
[179] M. Khuili, N. Fazouan, H.A. El Makarim, G. El Halani, E.H. Atmani, Comparative first principles study of ZnO doped with group III elements, J. Alloys Compd. 688 (2016) 368–375. doi:10.1016/j.jallcom.2016.06.294.
[180] M. Coll, J. Fontcuberta, M. Althammer, M. Bibes, H. Boschker, A. Calleja, G. Cheng, M. Cuoco, R. Dittmann, B. Dkhil, I. El Baggari, M. Fanciulli, I. Fina, E. Fortunato, C. Frontera, S. Fujita, V. Garcia, S.T.B. Goennenwein, C.-G. Granqvist, J. Grollier, R. Gross, A. Hagfeldt, G. Herranz, K. Hono, E. Houwman, M. Huijben, A. Kalaboukhov, D.J. Keeble, G. Koster, L.F. Kourkoutis, J. Levy, M. Lira-Cantu, J.L. MacManus-Driscoll, J. Mannhart, R. Martins, S. Menzel, T. Mikolajick, M. Napari, M.D. Nguyen, G. Niklasson, C. Paillard, S. Panigrahi, G. Rijnders, F. Sánchez, P. Sanchis, S. Sanna, D.G. Schlom, U. Schroeder, K.M. Shen, A. Siemon, M. Spreitzer, H. Sukegawa, R. Tamayo, J. van den Brink, N. Pryds, F.M. Granozio, Towards Oxide Electronics: a Roadmap, Appl. Surf. Sci. 482 (2019) 1–93. doi:10.1016/j.apsusc.2019.03.312.
[181] U. Özgür, D. Hofstetter, H. Morkoç, ZnO Devices and Applications: A Review of Current Status and Future Prospects, Proc. IEEE. 98 (2010) 1255–1268. doi:10.1109/JPROC.2010.2044550.
[182] D. Look, B. Claflin, Y. Alivov, S. Park, The future of ZnO light emitters, Phys. Status Solidi. 201 (2004) 2203–2212. http://mse.gist.ac.kr/~master/publication/data/DCLOOK.pdf (accessed October 8, 2015).
[183] Y.I. Alivov, J.E. Van Nostrand, D.C. Look, M. V. Chukichev, B.M. Ataev, Observation of 430 nm electroluminescence from ZnO/GaN heterojunction light-emitting diodes, Appl. Phys. Lett. 83 (2003) 2943–2945. doi:10.1063/1.1615308.
[184] D.J. Rogers, F. Hosseini Teherani, A. Yasan, K. Minder, P. Kung, M. Razeghi,

Electroluminescence at 375nm from a ZnO⁄GaN:Mg⁄c-Al2O3 heterojunction light emitting diode, Appl. Phys. Lett. 88 (2006) 141918. doi:10.1063/1.2195009.
[185] D. Rogers, F.H. Teherani, P. Kung, K. Minder, M. Razeghi, Materials characterization of n - ZnO / p - GaN : Mg / c - Al2O3 UV LEDs grown by pulsed laser deposition and metal–organic chemical vapor deposition, Superlattices Microstruct. 42 (2007) 322–326. doi:10.1016/j.spmi.2007.04.075.
[186] D.J. Rogers, F.H. Teherani, V.E. Sandana, M. Razeghi, ZnO thin films and nanostructures for emerging optoelectronic applications, in: L.A. Eldada, E.-H. Lee (Eds.), 2010: p. 76050K. doi:10.1117/12.862634.
[187] C. Bayram, M. Razeghi, D.J. Rogers, F.H. Teherani, Fabrication and characterization of novel hybrid green light emitting diodes based on substituting n-type ZnO for n-type GaN in an inverted p-n junction, J. Vac. Sci. Technol. B Microelectron. Nanom. Struct. 27 (2009) 1784. doi:10.1116/1.3116590.
[188] D.J. Rogers, F. Hosseini Teherani, A. Ougazzaden, S. Gautier, L. Divay, A. Lusson, O. Durand, F. Wyczisk, G. Garry, T. Monteiro, M.R. Correira, M. Peres, A. Neves, D. McGrouther, J.N. Chapman, M. Razeghi, Use of ZnO thin films as sacrificial templates for metal organic vapor phase epitaxy and chemical lift-off of GaN, Appl. Phys. Lett. 91 (2007) 071120. doi:10.1063/1.2770655.
[189] Y.I. Alivov, E. V. Kalinina, A.E. Cherenkov, D.C. Look, B.M. Ataev, A.K. Omaev, M. V. Chukichev, D.M. Bagnall, Fabrication and characterization of n-ZnO/p-AlGaN heterojunction light-emitting diodes on 6H-SiC substrates, Appl. Phys. Lett. 83 (2003) 4719–4721. doi:10.1063/1.1632537.
[190] F. Schuster, B. Laumer, R.R. Zamani, C. Magén, J.R. Morante, J. Arbiol, M. Stutzmann, p-GaN/n-ZnO Heterojunction Nanowires: Optoelectronic Properties and the Role of Interface Polarity, ACS Nano. 8 (2014) 4376–4384. doi:https://doi.org/10.1021/nn406134e.
[191] F. Fresno, R. Portela, S. Sú Arez, J.M. Coronado, Photocatalytic materials: recent achievements and near future trends, J. Mater. Chem. A. 2 (2014) 2863–2884. doi:10.1039/c3ta13793g.
[192] M.Y. Guo, A.M.C. Ng, F. Liu, A.B. Djurišić, W.K. Chan, H. Su, K.S. Wong, Effect of Native Defects on Photocatalytic Properties of ZnO, J. Phys. Chem. C. 115 (2011) 11095–11101. doi:10.1021/jp200926u.
[193] T. Reimer, I. Paulowicz, R. Röder, S. Kaps, O. Lupan, S. Chemnitz, W. Benecke, C. Ronning, R. Adelung, Y.K. Mishra, Single step integration of ZnO Nano-and microneedles in Si trenches by novel flame transport approach: Whispering gallery modes and photocatalytic properties, ACS Appl. Mater. Interfaces. 6 (2014) 7806–7815. doi:10.1021/am5010877.
[194] C.B. Ong, L.Y. Ng, A.W. Mohammad, A review of ZnO nanoparticles as solar photocatalysts: Synthesis, mechanisms and applications, Renew. Sustain. Energy Rev. 81 (2018) 536–551. doi:10.1016/j.rser.2017.08.020.
[195] M. Pirhashemi, A. Habibi-Yangjeh, S. Rahim Pouran, Review on the criteria anticipated for the fabrication of highly efficient ZnO-based visible-light-driven photocatalysts, J. Ind. Eng. Chem. 62 (2018) 1–25. doi:10.1016/j.jiec.2018.01.012.
[196] C. Hariharan, Photocatalytic degradation of organic contaminants in water by ZnO nanoparticles: Revisited, Appl. Catal. A Gen. 304 (2006) 55–61. doi:10.1016/J.APCATA.2006.02.020.
[197] J.M. Coronado, F. Fresno, M.D. Hernández-Alonso, R. Portela, eds., Design of Advanced Photocatalytic Materials for Energy and Environmental Applications, Springer London, London, 2013. doi:10.1007/978-1-4471-5061-9.

[198] N. Kislov, J. Lahiri, H. Verma, D.Y. Goswami, E. Stefanakos, M. Batzill, Photocatalytic Degradation of Methyl Orange over Single Crystalline ZnO: Orientation Dependence of Photoactivity and Photostability of ZnO, Langmuir. 25 (2009) 3310–3315. doi:10.1021/la803845f.

[199] M.J. Height, S.E. Pratsinis, O. Mekasuwandumrong, P. Praserthdam, Ag-ZnO catalysts for UV-photodegradation of methylene blue, Appl. Catal. B Environ. 63 (2006) 305–312. doi:10.1016/j.apcatb.2005.10.018.

[200] E. Fortunato, A. Gonçalves, A. Pimentel, P. Barquinha, G. Gonçalves, L. Pereira, I. Ferreira, R. Martins, Zinc oxide, a multifunctional material: from material to device applications, Appl. Phys. A. 96 (2009) 197–205. doi:10.1007/s00339-009-5086-5.

[201] S. Baruah, S.S. Sinha, B. Ghosh, S.K. Pal, A.K. Raychaudhuri, J. Dutta, Photoreactivity of ZnO nanoparticles in visible light: Effect of surface states on electron transfer reaction, J. Appl. Phys. 105 (2009) 074308. doi:10.1063/1.3100221.

[202] R. Ullah, J. Dutta, Photocatalytic degradation of organic dyes with manganese-doped ZnO nanoparticles., J. Hazard. Mater. 156 (2008) 194–200. doi:10.1016/j.jhazmat.2007.12.033.

[203] A.B. Djurišić, Y.H. Leung, A.M. Ching Ng, Strategies for improving the efficiency of semiconductor metal oxide photocatalysis, Mater. Horizons. 1 (2014) 400. doi:10.1039/c4mh00031e.

[204] F. Liu, Y.H. Leung, A.B. Djurišić, A.M.C. Ng, W.K. Chan, K.L. Ng, K.S. Wong, C. Liao, K. Shih, C. Surya, Effect of Plasma Treatment on Native Defects and Photocatalytic Activities of Zinc Oxide Tetrapods, J. Phys. Chem. C. 118 (2014) 22760–22767. doi:10.1021/jp506468r.

[205] V. Vamathevan, R. Amal, D. Beydoun, G. Low, S. McEvoy, Photocatalytic oxidation of organics in water using pure and silver-modified titanium dioxide particles, J. Photochem. Photobiol. A Chem. 148 (2002) 233–245. doi:10.1016/S1010-6030(02)00049-7.

[206] A.C. Dodd, A.J. McKinley, M. Saunders, T. Tsuzuki, Effect of Particle Size on the Photocatalytic Activity of Nanoparticulate Zinc Oxide, J. Nanoparticle Res. 8 (2006) 43–51. doi:10.1007/s11051-005-5131-z.

[207] S.J. Park, G.S. Das, F. Schütt, R. Adelung, Y.K. Mishra, K.M. Tripathi, T. Kim, Visible-light photocatalysis by carbon-nano-onion-functionalized ZnO tetrapods: degradation of 2,4-dinitrophenol and a plant-model-based ecological assessment, NPG Asia Mater. 11 (2019) 8. doi:10.1038/s41427-019-0107-0.

[208] J. Xu, K. Fan, W. Shi, K. Li, T. Peng, Application of ZnO micro-flowers as scattering layer for ZnO-based dye-sensitized solar cells with enhanced conversion efficiency, Sol. Energy. 101 (2014) 150–159. doi:10.1016/j.solener.2013.12.039.

[209] A. Hagfeldt, G. Boschloo, L. Sun, L. Kloo, H. Pettersson, Dye-Sensitized Solar Cells, Chem. Rev. 110 (2010) 6595–6663. doi:10.1021/cr900356p.

[210] H. Gerischer, Electrochemical techniques for the study of photosensitization, Photochem. Photobiol. 16 (2008) 243–260. doi:10.1111/j.1751-1097.1972.tb06296.x.

[211] H. Tributsch, M. Calvin, Electrochemistry of exvited molecules: photoelectrochemical reactions of chlorophylls, Photochem. Photobiol. 14 (1971) 95–112. doi:10.1111/j.1751-1097.1971.tb06156.x.

[212] J.A. Anta, E. Guillén, R. Tena-Zaera, ZnO-Based Dye-Sensitized Solar Cells, J. Phys. Chem. C. 116 (2012) 11413–11425. doi:10.1021/jp3010025.

[213] C.-P. Lee, C.-Y. Chou, C.-Y. Chen, M.-H. Yeh, L.-Y. Lin, R. Vittal, C.-G. Wu, K.-C. Ho, Zinc oxide-based dye-sensitized solar cells with a ruthenium dye containing an alkyl bithiophene group, J. Power Sources. 246 (2014) 1–9. doi:10.1016/j.jpowsour.2013.05.101.
[214] Q. Zhang, C.S. Dandeneau, X. Zhou, G. Cao, ZnO Nanostructures for Dye-Sensitized Solar Cells, Adv. Mater. 21 (2009) 4087–4108. doi:10.1002/adma.200803827.
[215] M.M. Mohamed, M.A. Ghanem, S.M. Reda, M. Khairy, E.M. Naguib, N.H. Alotaibi, Photovoltaic and capacitance performance of low-resistance ZnO nanorods incorporated into carbon nanotube-graphene oxide nanocomposites, Electrochim. Acta. 307 (2019) 430–441. doi:10.1016/j.electacta.2019.03.226.
[216] D. Calestani, M. Zha, R. Mosca, A. Zappettini, M.C. Carotta, V. Di Natale, L. Zanotti, Growth of ZnO tetrapods for nanostructure-based gas sensors, Sensors Actuators B Chem. 144 (2010) 472–478. doi:10.1016/j.snb.2009.11.009.
[217] C. Xiangfeng, J. Dongli, A. B.Djurišic, Y.H. Leung, Gas-sensing properties of thick film based on ZnO nano-tetrapods, Chem. Phys. Lett. 401 (2005) 426–429. doi:https://doi.org/10.1016/j.cplett.2004.11.091.
[218] S. Rodriguez-Mozaz, M.J.L. de Alda, D. Barceló, Biosensors as useful tools for environmental analysis and monitoring, Anal. Bioanal. Chem. 386 (2006) 1025–1041.
[219] J. Hahm, Fundamental Properties of One-Dimensional Zinc Oxide Nanomaterials and Implementations in Various Detection Modes of Enhanced Biosensing, Annu. Rev. Phys. Chem. 67 (2016) 691–717. doi:10.1146/annurev-physchem-031215-010949.
[220] S.S. Bhat, A. Qurashi, F.A. Khanday, ZnO nanostructures based biosensors for cancer and infectious disease applications: Perspectives, prospects and promises, TrAC - Trends Anal. Chem. 86 (2017) 1–13. doi:10.1016/j.trac.2016.10.001.
[221] R. Yakimova, ZnO materials and surface tailoring for biosensing, Front. Biosci. E4 (2012) 254. doi:10.2741/374.
[222] A.A. Ansari, A. Kaushik, P.R. Solanki, B.D. Malhotra, Nanostructured zinc oxide platform for mycotoxin detection, Bioelectrochemistry. 77 (2010) 75–81. doi:10.1016/j.bioelechem.2009.06.014.
[223] R. Viter, V. Khranovskyy, N. Starodub, Y. Ogorodniichuk, S. Gevelyuk, Z. Gertnere, N. Poletaev, R. Yakimova, D. Erts, V. Smyntyna, A. Ubelis, Application of Room Temperature Photoluminescence From ZnO Nanorods for Salmonella Detection, IEEE Sens. J. 14 (2014) 2028–2034. doi:10.1109/JSEN.2014.2309277.
[224] J.X. Wang, X.W. Sun, A. Wei, Y. Lei, X.P. Cai, C.M. Li, Z.L. Dong, Zinc oxide nanocomb biosensor for glucose detection, Appl. Phys. Lett. 88 (2006) 233106. doi:10.1063/1.2210078.
[225] S.N. Sarangi, S. Nozaki, S.N. Sahu, ZnO Nanorod-Based Non-Enzymatic Optical Glucose Biosensor, J. Biomed. Nanotechnol. 11 (2015) 988–996. doi:10.1166/jbn.2015.2048.
[226] Y.-M. Lu, P.-C. Wang, J.-F. Tang, S.-Y. Chu, Dependence of seed layer thickness on sensitivity of nano-ZnO cholesterol biosensor, IOP Conf. Ser. Mater. Sci. Eng. 167 (2017) 012021. doi:10.1088/1757-899X/167/1/012021.
[227] L. Zheng, Y. Wan, P. Qi, Y. Sun, D. Zhang, L. Yu, Lectin functionalized ZnO nanoarrays as a 3D nano-biointerface for bacterial detection, Talanta. 167 (2017) 600–606. doi:10.1016/j.talanta.2017.03.007.
[228] S. Kumar, W. Ahlawat, R. Kumar, N. Dilbaghi, Graphene, carbon nanotubes,

zinc oxide and gold as elite nanomaterials for fabrication of biosensors for healthcare, Biosens. Bioelectron. 70 (2015) 498–503. doi:10.1016/j.bios.2015.03.062.

[229] N.R. Shanmugam, S. Muthukumar, A.P. Selvam, S. Prasad, Electrochemical nanostructured ZnO biosensor for ultrasensitive detection of cardiac troponin-T, Nanomedicine. 11 (2016) 1345–1358. doi:10.2217/nnm-2016-0048.

[230] P.R. Solanki, A. Kaushik, A.A. Ansari, B.D. Malhotra, Nanostructured zinc oxide platform for cholesterol sensor, Appl. Phys. Lett. 94 (2009) 143901. doi:https://doi.org/10.1063/1.3111429.

[231] J. Ghosh, R. Ghosh, P.K. Giri, Tuning the visible photoluminescence in Al doped ZnO thin film and its application in label-free glucose detection, Sensors Actuators B Chem. 254 (2018) 681–689. doi:http://dx.doi.org/10.1016/j.snb.2017.07.110.